TU/e EINDHOVEN UNIVERSITY OF TECHNOLOGY

Transitional free convection flows induced by thermal line sources

Citation for published version (APA):
Bastiaans, R. J. M. (1993). *Transitional free convection flows induced by thermal line sources.* (EUT report. W, Dept. of Mechanical Engineering; Vol. 93-W-002). Eindhoven University of Technology.

Document status and date:
Published: 01/01/1993

Document Version:
Publisher's PDF, also known as Version of Record (includes final page, issue and volume numbers)

Please check the document version of this publication:

• A submitted manuscript is the version of the article upon submission and before peer-review. There can be important differences between the submitted version and the official published version of record. People interested in the research are advised to contact the author for the final version of the publication, or visit the DOI to the publisher's website.
• The final author version and the galley proof are versions of the publication after peer review.
• The final published version features the final layout of the paper including the volume, issue and page numbers.

Link to publication

General rights
Copyright and moral rights for the publications made accessible in the public portal are retained by the authors and/or other copyright owners and it is a condition of accessing publications that users recognise and abide by the legal requirements associated with these rights.

• Users may download and print one copy of any publication from the public portal for the purpose of private study or research.
• You may not further distribute the material or use it for any profit-making activity or commercial gain
• You may freely distribute the URL identifying the publication in the public portal.

If the publication is distributed under the terms of Article 25fa of the Dutch Copyright Act, indicated by the "Taverne" license above, please follow below link for the End User Agreement:

www.tue.nl/taverne

Take down policy
If you believe that this document breaches copyright please contact us at:

openaccess@tue.nl

providing details and we will investigate your claim.

Download date: 04. Oct. 2023

Transitional free convection flows induced by thermal line sources

Rob J.M. Bastiaans

Eindhoven University of Technology
Research Reports
ISSN 0167-9708 CODEN: TEUEDE

EUT Report 93-W-002

July 1993

CIP-GEGEVENS KONINKLIJKE BIBLIOTHEEK, DEN HAAG

Bastiaans, Rob J.M.

Transitional free convection flows induced by thermal line sources / Rob J.M. Bastiaans. - Eindhoven : Eindhoven University of Technology. - Ill. - (Eindhoven University of Technology research reports, ISSN 0167-9708 ; EUT report 93-W-002)
With ref.
ISBN 90-386-0302-9
Subject headings: transitional flows / line heat sources / large-eddy simulation.

ISBN 90-386-0302-9
©Eindhoven University of Technology, Eindhoven, 1993.

Transitional free convection flows induced by thermal line sources / Rob J.M. Bastiaans. - Eindhoven : Eindhoven University of Technology, 1993. - viii, 61 p. - (Eindhoven University of Technology Research Reports, ISSN 0167-9708, EUT Report 93-W-002). - ISBN 90-386-0302-9

Abstract

In the present study the usefullness of a large eddy simulation for transition is examined. Numerical results of such simulations are presented from a study to determine the characteristics of a flow induced by a thermal line source. The first bifurcation to time dependent motion and the route to chaos are considered. Qualitatively these features are in good agreement with theory.

The governing equations, the concept of large eddy simulation and the numerical code that was used are described extensively. Also the results from a literature survey are presented. Special attention is paid to analytical solutions for the boundary layer equations for laminar flow and the stability of these solutions. It includes also overall conservation principles for turbulent plumes and results obtained by experiments.

Keywords

Transitional flows, Line heat source, Large-Eddy simulation

Author's Affiliation

J.M. Burgers Centre for Fluid Mechanics
Eindhoven University of Technology
Department of Mechanical Engineering
Energy Technology Division
P.O. Box 513
5600 MB Eindhoven
The Netherlands

Preface

This report deals with a preliminary investigation of the characteristics of natural convection flows. The intention is to find a numerical model that can describe physical reality with good accuracy. Therefore a large eddy simulation technique will be used. Application of this method is not trivial for both transitional flows and complex geometries. The final objective is to find a large eddy model implemented in a numerical code that can deal with these problems.

Natural convection occurs when a local heating of a fluid causes it to rise due to buoyancy effects. At a low heating rate the flow will be laminar. As the buoyancy effects are growing an oscillating flow will occur getting more complex and finally becoming chaotic or turbulent. In case of a turbulent plume a spatial transition from laminar to turbulent flow will appear.

First a literature survey is described dealing with analytical theories of laminar and turbulent plumes. Also a stability analysis is included. Experiments are quoted in which the transition of buoyant plumes is investigated.

Later on some large eddy simulations were performed for transitional flows in cubical flow domains. The conclusions from these calculations form the point of departure of further more thorough investigations, both numerical and experimental. The used numerical code was made available by Prof. F.T.M. Nieuwstadt and T.A.M. Versteegh from Delft University of Technology for which they are very much acknowledged. They are also thanked for a three month stay of the author of this report at Delft University.

Rob Bastiaans

9th July 1993

Contents

Chapter 1

Problem definition

1.1 Introduction

In many process engineering problems heat exchange takes place in combination with turbulent flows. An example of such a problem is the process of natural convection in the heat storage vessel of a solar energy water system or the plumes induced by hot electronic components in various devices. In most cases the design of these systems is based on empirical relationships and analytical solutions of strongly simplified problems. The reason for applying these kinds of treatments is because of the complexity of both the geometries considered (3D-effects) and the flow phenomena, more or less as a consequence of that (areas of separation, secondary flows, turbulence). Therefore the designing process, in the case of non-trivial geometries, is still a rather tricky business.

One of the things that are needed to optimize the dimensions of the devices as mentioned above is the necessity of the development of a physical correct numerical code in order to simulate the turbulent flow and heat exchange in complicated flow configurations. After numerical analysis and experimental validation, the findings have to be translated in a relative simple model with an accuracy that is convenient within the designing proces. In this way it is possible to deduce important information about designing rules for the benefit of the in detail optimized design of apparatus in which turbulent natural convection flows occur. In the next sections of this chapter the problem under consideration will be defined more extensively. Also the general approach to solve the problem will be outlined.

1.2 Natural convection

In this study a rather small hot object is considered. This body is surrounded by a relative large amount of fluid. The domain under consideration thus is large with respect to the dimensions of the heat source. Conduction is the initial transport mechanism of the heat exchange. The fluid near to the heat source gets warm and due to the interaction of density differences with the gravity field a convective flow sets in. A convective flow that is forced by buoyancy is called natural or free convection, in contrast to a forced convective flow, where a pressure gradient drives the flow. The convective heat transport mechanism or advection is much more effective than conduction without flow. In the former case the temperature gradients are much larger implying conduction to be more efficient, resulting in a larger heat flux.

The rate of advection can be expressed by the Grashof number, $Gr = \frac{g\beta\Delta TL^3}{\nu^2}$, a dimensionless parameter expressing the ratio of the product of buoyancy and inertia forces to viscous forces squared. Given the geometry, the Grashof number and the physical properties of the fluid, expressed by the Prandtl number, $Pr = \frac{\nu}{\kappa}$, the process is fully determined. Exceeding a critical Grashof number generally results in a periodic oscillating flow. In this case hydrodynamic instability arises in a laminar flow when a balance of buoyancy, pressure and viscous forces may contribute net energy to a disturbance, causing it to grow as it is convected along. A further increasing of the forcing leads to a chaotic motion that is called turbulence, a word introduced by Lord Kelvin. The intensity of the turbulent motion still depends on the Grashof number. The area in which the flow regime is turbulent is limited to a thermal plume above the heated body.

1.3 Thermal line source

As a first approach to describe the transport processes that occur in the mentioned types of devices we'll consider an infinitely long horizontal line heat source. Figure 1.1 shows the geometry and coordinate system that is used. Analytical considerations and solutions of the resulting equations for these flows are described in chapter 3. In the laminar case, at low Grashof numbers, a plane plume will develop. A flow of this type in an infinite space can be analyzed by applying boundary layer assumptions. Transition can be studied by perturbing the basic laminar flow by small two-dimensional velocity and temperature disturbances.

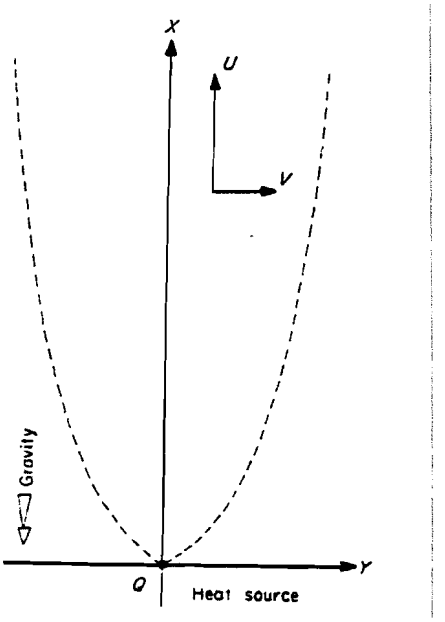

Figure 1.1: Thermal line source; definition of geometry and coordinate system

The general approach in the analysis of turbulent plumes is to consider the conservation principles for the overall mass, momentum and energy in the flow. Experimental information for the modelling of the mean flow is often employed. The process of entrainment, or mixing,

of the ambient fluid into the flow is important in all free boundary turbulent flows. An important approximation is that the mean inflow, or entrainment velocity at the edge of the boundary layer, is proportional to the local mean vertical velocity. The entrainment coefficient is usually determined experimentally.

The analytical methods as mentioned above are all more or less verified experimentally. The advantage of these methods is that there are very few parameters and every variation of these parameters is rather easy to calculate. This approach on the other hand can only be used in the most simple cases.

Our goal is to simulate these flows, especially the transitional and turbulent ones, with a numerical code in such a way that a sufficient accurate description of the heat transfer processes can be obtained. By considering these elementary geometries it is possible to verify the code with data that are generated both analytically and experimentally. In the research stadium later on the code could be used to solve more complex problems. For solving these problems an analytical approach is no longer applicable. Experimental validation is the way to test the code under these circumstances.

1.4 Large eddy simulation

One of the main characteristics of turbulence is the structure of the flow. The structure of a turbulent fluid is build up out of many scales of vortical motion. The macroscopical scales on the one hand depend mainly on the geometry of the domain under consideration. The microscopic scales are mainly influenced by molecular processes, like the action of viscosity. In the inertial subrange, kinetic energy is transported continuously from the large scales to the small ones in which it is dissipated to heat.

Because of this the numerical grid must have a resolution that has to be very high to resolve the smallest whirls. There is theoretical prove that in forced convective flows the number of computational nodes has to be proportional to $Re^{9/4}$. In natural convection flows it is observed, e.g. by Kotsovinos [22], that most of the intensity of the turbulent fluctuations of the temperature and velocity field is contained in the low wave number range. This range corresponds with the larger scales and this means that the required amount of gridpoints is somewhat smaller in natural convection problems. To solve the most common flows, that are the turbulent ones, we would need a computer effort that is far beyond the scope of the capacity of modern supercomputers. As a consequence of that the problem has to be solved in a slightly different manner. "Large eddy simulation" (L.E.S.) a technique developed by scientists working in the field of meteorology can provide a way out. The approach of this method is outlined in chapter 4.

Using L.E.S. the Navier-Stokes equations are spatially filtered with a filterlength that is at the same time much larger than the smallest scales and much smaller than the macroscopic scales of turbulent motion. A model has to be made to correct for the influence of the scales of motion that are filtered out. The resulting equations can be numerically solved to get a solution for the structure of the motion down to the scale of the distances between the nodes, the so called large eddies.

1.5 Main topics of investigation

As mentioned in the previous sections it is our aim to create a possibility to optimize the design of several devices in which natural convection occurs. To do this we will start with numerical simulation of flows induced by thermal line sources. The numerical code we start with is based on a finite difference method of discretizing the Navier-Stokes equations. This code will be clarified in chapter 5. With the numerical code we want to test several models for balancing the subgrid scale influences in turbulent free convection flow configurations, i.e. when a spatial transition from laminar to turbulent flow occurs. To calculate accurately all occurring effects also a temporal flow transition should be predicted fairly well.

First, transition processes will be calculated with the existing subgrid closure, as described in chapter 5. The characteristics of the calculated flow, induced by a thermal line source have to be studied. The first bifurcation to time dependent motion and the route to chaos are considered. Also attention will be given to the topology of the simulated flows. In a later stadium these characteristics will be compared to those obtained by experiments.

Chapter 2

Governing equations

2.1 Navier-Stokes equations

The equations that are commonly used to describe the flow variables in the continuum approach consist of a set of conservation laws and are normally referred to as the Navier-Stokes equations. It contains a continuity equation wherein conservation of mass is prescribed and Newton's second law for the conservation of momentum. It is assumed that the density and viscosity are invariant in space and time and that we are dealing with a Newtonian fluid, i.e. a medium in which the constitutional law holds that shear stress is linear proportional to strain. This system, written in a Cartesian coordinate system and using Einstein's convention, i.e. summing over repeated indices, reads:

$$\frac{\partial u_i}{\partial x_i} = 0 \tag{2.1}$$

$$\frac{\partial u_i}{\partial t} + \frac{\partial}{\partial x_j}(u_i u_j) = f_i - \frac{1}{\rho}\frac{\partial p}{\partial x_i} + \nu \frac{\partial^2 u_i}{\partial x_j \partial x_j} \tag{2.2}$$

where u_i is the velocity vector, p the pressure, ρ the density, ν the kinematic viscosity and f_i an additional body force. These equations in combination with appropriate boundary and initial conditions describe the flow for all later times.

2.2 The Boussinesq approximation

In the cases considered the body force only contains a buoyant term. Density differences only occur in this term as a first approximation, in all other terms the variation of the density is neglected, hence:

$$f_i = \frac{(\rho - \rho_0)}{\rho_0} g_i \tag{2.3}$$

in which g_i only has a non-zero value $-g$ in the vertical direction. The density ρ_0 is defined as some reference density.

A further simplification is the linearization of the temperature dependency of the density, referred to as the Boussinesq approximation, in which the density is expanded into a Taylor series around a reference temperature T_0 (at which $\rho(T_0) = \rho_0$) and truncated after the second

term:

$$\rho = \rho_0 + (T - T_0) \left.\frac{\partial \rho}{\partial T}\right|_{T=T_0} \tag{2.4}$$

Defining a coefficient of thermal expansion $\beta_0 = \beta(T_0)$ at constant pressure:

$$\beta_0 = -\frac{1}{\rho_0} \left.\frac{\partial \rho}{\partial T}\right|_{T=T_0} \tag{2.5}$$

we can write the momentum equation as:

$$\frac{\partial u_i}{\partial t} + \frac{\partial}{\partial x_j}(u_i u_j) = -\beta_0 (T - T_0) g_i - \frac{1}{\rho_0}\frac{\partial p}{\partial x_i} + \nu_0 \frac{\partial^2 u_i}{\partial x_j \partial x_j} \tag{2.6}$$

Since we have now introduced the temperature as a new variable in our system of equations, an additional expression for solving the temperature is required. To determine the temperature as function of space and time we apply the first law of thermodynamics for conserving energy:

$$\frac{\partial T}{\partial t} + \frac{\partial}{\partial x_j}(u_j T) = \kappa_0 \frac{\partial^2 T}{\partial x_j \partial x_j} \tag{2.7}$$

in which the thermal diffusivity κ_0 is defined and assumed to be constant. The energy equation in the form as written above does not account for the action of radiation and viscous dissipation. Fourier's constitutional law is used to relate the temperature gradient to the heat flux density. It is also assumed that the ratio of pressure work forces to convection forces is very low[1].

2.3 The non-dimensional form of Boussinesq's formulation

All variables can be non-dimensionalized with a characteristic velocity scale U, representative for the mean flow velocity and a length scale L proportional to a characteristic length of the flow domain. Scaling of the temperature can be done by using a temperature difference ΔT and time can be scaled with a characteristic frequency ω. The pressure is non-dimensionalized with ρU^2. The Navier-Stokes equations in the Boussinesq formulation then read:

$$\frac{\partial u_i}{\partial x_i} = 0 \tag{2.8}$$

$$Sr \frac{\partial u_i}{\partial t} + \frac{\partial}{\partial x_j}(u_i u_j) = \frac{Gr}{Re^2}(T - T_0)\delta_{i3} - \frac{\partial p}{\partial x_i} + \frac{1}{Re}\frac{\partial^2 u_i}{\partial x_j^2} \tag{2.9}$$

$$Sr \frac{\partial T}{\partial t} + \frac{\partial}{\partial x_j}(u_j T) = \frac{1}{RePr}\frac{\partial^2 T}{\partial x_j^2} \tag{2.10}$$

in which the following dimensionless groups can be distinguished:

$$Sr = \frac{\omega L}{U} \tag{2.11}$$

[1] see Sillekens [38].

the Strouhal number to express the ratio of instationary to inertia forces,

$$Gr = \frac{g\beta\Delta T L^3}{\nu^2} \tag{2.12}$$

the Grashof number which is the ratio of the product of buoyancy and inertia forces to viscous forces squared,

$$Re = \frac{UL}{\nu} \tag{2.13}$$

the Reynolds number expressing the ratio of inertia to viscous forces, and

$$Pr = \frac{\nu}{\kappa} \tag{2.14}$$

the Prandtl number giving the ratio of molecular momentum diffusivity to thermal diffusivity.

2.4 Validity of the Boussinesq formulation

In determining the governing equations for the flows considered we made some assumptions and approximations. The source of the major inaccuracies lies in the fact that the properties β, κ, ν and ρ are not constant. Since we are only considering water as the flow medium we'll look at the properties of water a little closer.

For the liquid water the pressure dependence of the mentioned properties is small and there is mainly a temperature dependence. Also the pressure variations are low in the interesting area of flow regimes so that it is no physical violence at all to neglect the pressure dependence. The temperature dependence is shown in figure 2.1 for the interesting temperature range. Gray and Giorgini [16] have investigated the validity of the Boussinesq formulation. They show that this formulation requires that the characteristic temperature differences ΔT are sufficiently small. As a concrete example they considered water at an average temperature of 15° C under atmospheric conditions. The requirement of less then 10 % error in the terms of the equations demands that $\Delta T < 1.25°$ C is satisfied. It is uncertain however what this means for the solution.

It can be concluded that the applicability of the Boussinesq formulation is strongly limited. Especially in the neighbourhood of $T_0 = 4°$ C where β goes to zero and changes sign, solutions of this formulation don't make sense anymore. It has to be investigated if β can be used in a temperature dependent manner and what the critical temperature difference will be in that case. Of course the temperature may still not vary more then 1.25° C between two collocation points of the numerical grid. It has to be remarked that in pure natural convection flows generally only a large temperature gradient exists near the heating body, in the rest of the flow domain there are only small temperature differences.

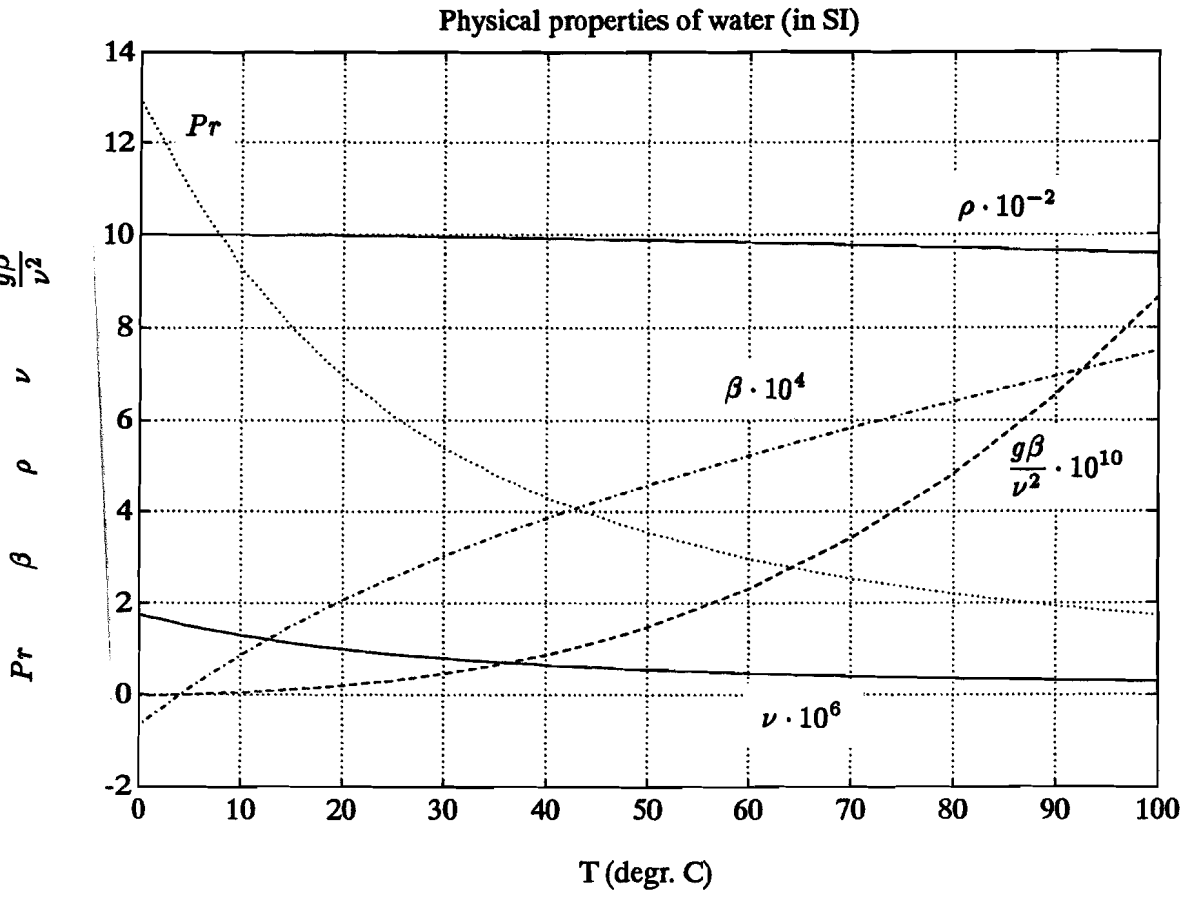

Figure 2.1: Temperature dependence of the physical properties of water

Chapter 3

Analytical solutions and experiments

3.1 Similarity equations

In this section the idealized problem of a laminar flow generated by a horizontal line heat source is discussed. In practice this flow would be approached by the flow arising from long tubes and thin wires. The idealized flow is attained also far downstream for finite-sized sources of arbitrary shape. Here we shall follow the derivation of Gebhart, Pera and Schorr [13] to solve the idealized flow problem.

The governing continuity, momentum and energy equations are simplified by the Boussinesq approximation and boundary layer assumptions to yield:

$$\frac{\partial u}{\partial x} + \frac{\partial v}{\partial y} = 0 \tag{3.1}$$

$$u\frac{\partial u}{\partial x} + v\frac{\partial u}{\partial y} = g\beta\Delta T + \nu\frac{\partial^2 u}{\partial y^2} \tag{3.2}$$

$$u\frac{\partial T}{\partial x} + v\frac{\partial T}{\partial y} = \kappa\frac{\partial^2 T}{\partial y^2} \tag{3.3}$$

in which the x-direction is vertical and the y-direction is horizontally oriented (see figure 1.1). These equations are solved by using a similarity variable $\eta(x,y)$ and a streamfuncion $\psi(x,y)$ (for which $u = \partial\psi/\partial y$ and $v = -\partial\psi/\partial x$) that can be derived by eliminating the x-dependence:

$$\eta = \frac{y}{x}\sqrt[4]{\frac{Gr_x}{4}} \tag{3.4}$$

$$\psi = 4\nu\sqrt[4]{\frac{Gr_x}{4}}f(\eta) \tag{3.5}$$

where:

$$Gr_x = \frac{g\beta x^3(T_0 - T_\infty)}{\nu^2} \tag{3.6}$$

is the local Grashof number. Indices 0 and ∞ stand for the midplane and undisturbed fluid and f is the nondimensional streamfunction.

The centerline temperature is initially assumed to be of a power law form:

$$T_0(x) - T_\infty = Nx^n \tag{3.7}$$

which will be shown to be appropriate. The dimensionless temperature $\phi(\eta)$ is defined as:

$$\phi(\eta) = \frac{T - T_\infty}{T_0 - T_\infty} \tag{3.8}$$

The continuity equation 3.1 is satisfied by ψ ($u = \partial\psi/\partial y$; $v = -\partial\psi/\partial x$) and 3.2 and 3.3 can be transformed using 3.4, 3.5, 3.7 and 3.8. Up to this point the analysis has been general for boundary layer flow over a vertical plate, plane sources and for plumes arising from horizontal line sources.

The total thermal energy convected in the boundary layer across any horizontal plane x in the plume is:

$$Q = \rho c_p \int_{-\infty}^{\infty} (T - T_\infty) u dy \tag{3.9}$$

and in similarity variables we get:

$$Q = 4\rho\nu c_p N \sqrt[4]{\frac{g\beta N}{4\nu^2}} x^{(5n+3)/4} \int_{-\infty}^{\infty} f'(\eta)\phi(\eta) d\eta \tag{3.10}$$

where N is defined in equation 3.7. Since Q is not a funcion of x, the value of n must be:

$$n = -\frac{3}{5} \tag{3.11}$$

Transforming the equations 3.1 and 3.3 and using this value for n the governing differential equations are obtained, giving:

$$f''' + \frac{12}{5} f f'' - \frac{4}{5} f'^2 + \phi = 0 \tag{3.12}$$

$$\phi'' + \frac{12}{5} Pr(f\phi)' = 0 \tag{3.13}$$

The five required boundary conditions can be generated from physical considerations as follows: The symmetry of the plume with respect to the midplane requires that $(\partial T/\partial y)_0 = 0$, $v_0 = 0$, $(\partial u/\partial y)_0 = 0$ and $T = T_0$. In terms of the similarity variables this reads:

$$\phi'(0) = f(0) = f''(0) = \phi(0) - 1 = 0 \tag{3.14}$$

All effects vanish at large values of η, i.e. $u \to 0$ and $T \to T_\infty$ giving:

$$f'(\infty) \to 0, \qquad \phi(\infty) \to 0 \tag{3.15}$$

The problem is not overdetermined since not all boundary conditions are independent: The second condition of 3.15 follows from the first. By integrating equation 3.13 we obtain:

$$\phi' + \frac{12}{5} Pr(f\phi) = C_1 \tag{3.16}$$

where the constant of integration C_1 is zero since $\phi'(0)$ and $f(0)$ are zero. Integrating again and using $\phi(0) = 1$ yields:

$$\phi(\eta) = e^{-\frac{12}{5}Pr\int_0^\eta f d\eta} \tag{3.17}$$

Since f is possitive and becomes constant for large η the dependence of the conditions 3.15 is demonstrated. The five independent conditions that may be used with the system of governing equations 3.12 and 3.13 are:

$$\phi'(0) = f(0) = f''(0) = \phi(0) - 1 = f'(\infty) = 0 \tag{3.18}$$

The two-dimensional plume flow is specified and by numerical integration solutions can be obtained for ϕ and f as functions of Pr.

3.2 Similarity solutions

Gebhart et al. [13] performed extensive numerical calculations in a Prandtl number range from 0.01 to 100. The streamfunction is plotted in figure 3.1. The distribution of the vertical

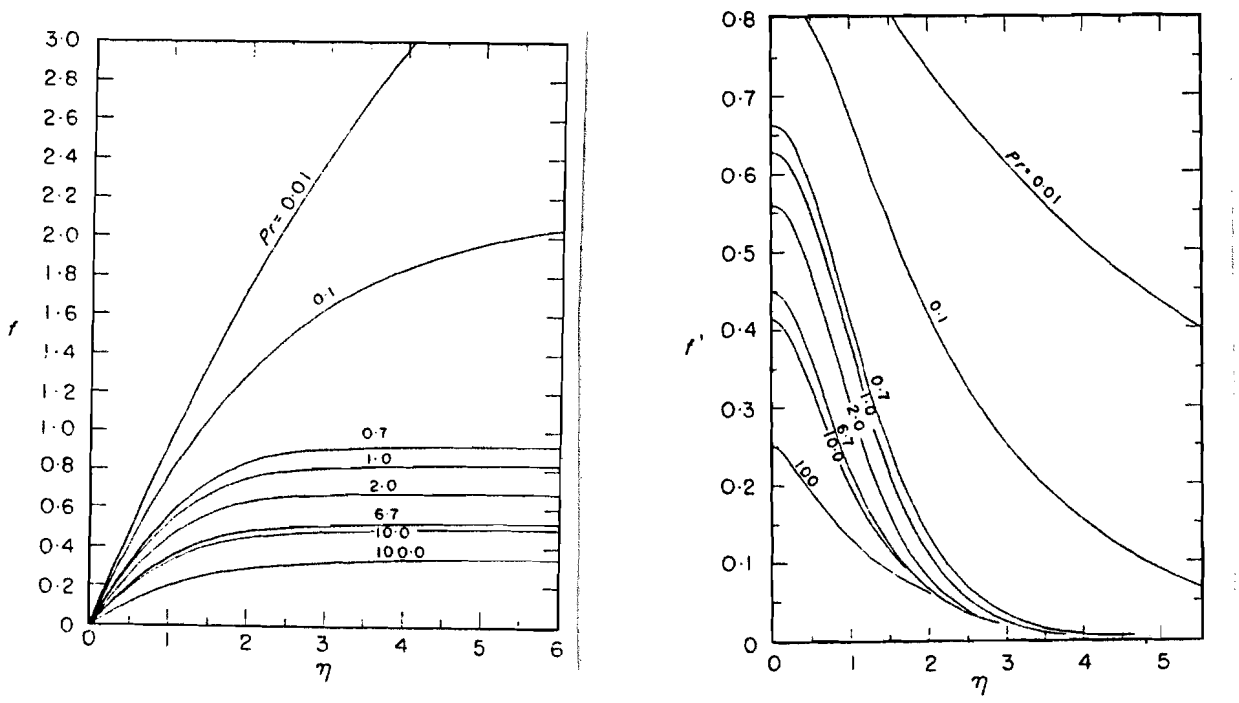

Figure 3.1: Streamfunction and velocity profiles as function of Pr, from Gebhart et al.

velocity component (that is linearly dependent on the derivative of the nondimensional streamfunction) and temperature are plotted in figures 3.1 and 3.2. Indications of the thickness of the temperature and velocity boundary regions can be obtained by considering $\phi(\eta) = 0.01$ and $u/u_{max} = f'(\eta)/f'(0) = 0.01$. For increasing Prandtl number the thermal layer becomes relatively much thinner than the velocity layer. In the case of air both boundary layers are of nearly the same thickness, i.e. $\eta \approx 3.3$, see appendix A.

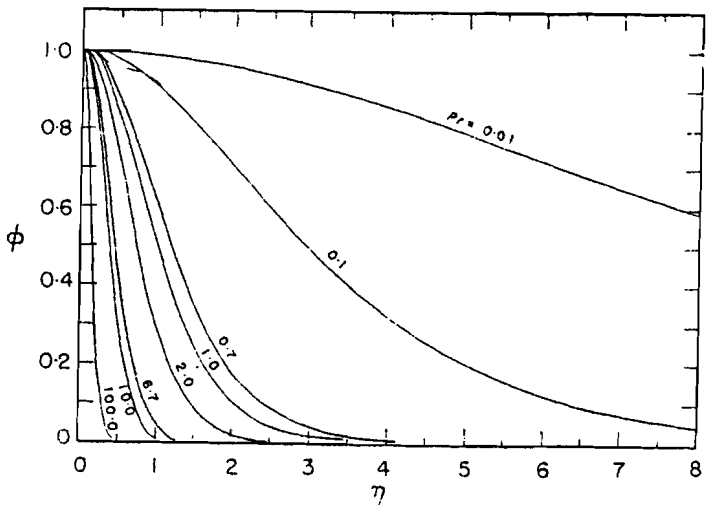

Figure 3.2: Temperature distribution as function of Pr, from Gebhart et al.

Now it is possible to calculate all other important variables. By defining:

$$I = \int_{-\infty}^{\infty} f'\phi d\eta \tag{3.19}$$

equation 3.10 can be written as:

$$N = \left(\frac{Q^4}{4^3 g\beta\nu^2\rho^4 c_p^4 I^4}\right)^{1/5} \tag{3.20}$$

which gives with 3.7 and 3.8 the temperature at any place in the field:

$$T = 4^{-3/5}\left(\frac{Q}{Ic_p}\right)^{4/5}\left(g\beta\rho^4\nu^2\right)^{-1/5} x^{-3/5}\phi(\eta) + T_\infty \tag{3.21}$$

The mass flow rate in the plume is given by:

$$\dot{m} = \int_{-\infty}^{\infty} \rho u dy = \left(\frac{64 g\beta\rho^4\nu^2 Q x^3}{c_p I}\right)^{1/5} J \tag{3.22}$$

where J is the value of the integral:

$$J = \int_{-\infty}^{\infty} f' d\eta \tag{3.23}$$

The velocity components are given by:

$$u = \left(\frac{2g\beta Q}{c_p I}\right)^{2/5}\left(\frac{x}{\rho^2\nu}\right)^{1/5} f'(\eta) \tag{3.24}$$

and

$$v = 4^{3/4}\frac{\nu}{x}Gr_x^{1/4}\left(\frac{2}{5}\eta f'(\eta) - \frac{3}{5}f(\eta)\right) \tag{3.25}$$

To determine the characteristics of the obtained flow field, calculations of velocity and temperature profiles at several constant x and y values are made. These profiles are depicted in figures 3.3, 3.4, 3.5 and 3.6 (x and y are according to the coordinate system as defined in the first chapter).

Also the temperature field is determined (figure 3.7) and compared to the interferogram obtained by Gebhart, Pera and Schorr [13] (line source with a heating rate of $Q = 51.89$ W/ms, in air at 25.7° C and atmospheric pressure), see figure 3.8. Figure 3.7 is obtained by calculating the temperature according to 3.21 in the same plane as the experiments are made. The temperature range of the outer fringe is comparable with the mentioned experiment, whereas the range of the inner fringe is much larger. The $f'(\eta)$ and $\phi(\eta)$ profiles were approximated by a Gaussian distribution fit, using the values at $\eta = 0$ obtained by Gebhart et al. [13]. These distributions are given in appendix A together with the resulting error function for f. The comparison shows that the boundary layer solution gives a plume thickness that is too small and the temperatures in the core and its gradient in x-direction are much too high. The discrepancy could be due to the fact that the comparison is made for an area that is too close to the source. The decrease of temperature with increase of height as is showed in figure 3.6 can also be seen in the fringe pattern, i.e. the fringes are closing at some height.

Experimental studies, reviewed by Jaluria [19] show a maximum temperature of 15-20 percent lower than the theoretically predicted centerline temperature. It is suggested that the difference is due to scattering of data caused by the swaying motion of the plume. Another point is the theoretically considered region $x \geq 0$ which implies no entrainment from below the source. If a horizontal plate is placed to obstruct entrainment from below, the centerline temperature has been observed to rise. A complication that arises here however is the introduction of a no-slip condition at the plate surface.

3.3 Stability of laminar plumes

The hydrodynamic stability of the laminar plume induced by a horizontal line source of heat was investigated by Pera and Gebhart [30]. Since two-dimensional disturbances are the least stable they considered only two-dimensional disturbances for the temperature distribution and the streamfunction superimposed upon the parallel base flow. These disturbances are characterized by $\omega_1 = 2\pi/\lambda$, the wavenumber of the disturbance, and its frequency ω_2:

$$e^{i(\omega_1 x - \omega_2 t)} \tag{3.26}$$

The imaginary part of ω_1 describes the amplification with respect to the x-coordinate and the imaginary part of ω_2 which is set to zero describes the amplification with time at fixed x.

In this way the traditional Orr-Sommerfeld equation is obtained with an additional coupling term, that arises from the buoyancy effect. Also a disturbance energy equation is obtained. With appropriate boundary conditions for symmetric and asymmetric disturbances the equations can be numerically integrated to determine the neutral stability curve, $\Im(\omega_1) = 0$. This was done for the inviscid asymptote (i.e. $Gr_x \to \infty$), the uncoupled case (i.e. neglecting the coupling terms of the perturbations) and the fully coupled form.

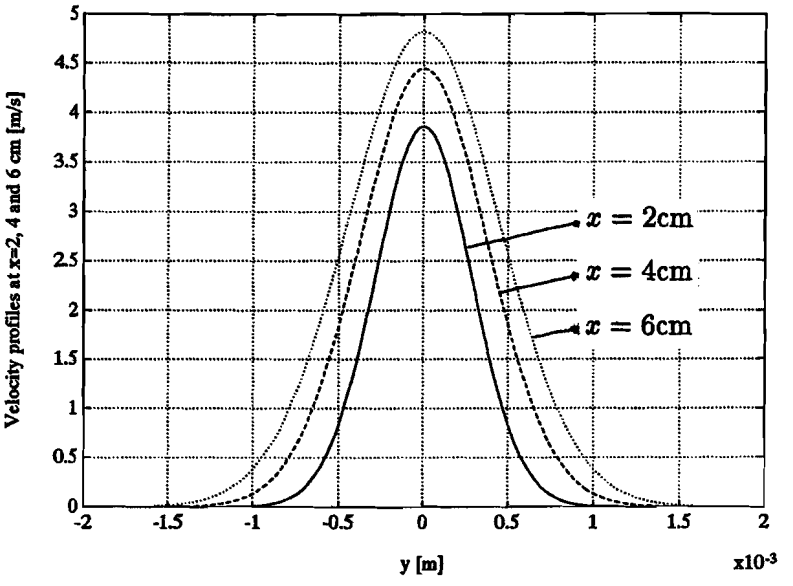

Figure 3.3: Velocity profiles at constant x

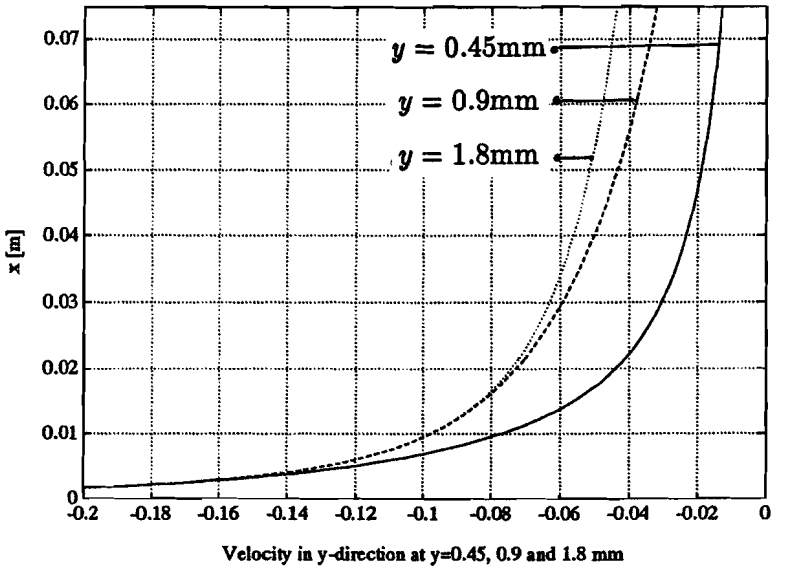

Figure 3.4: Velocity profiles at constant y

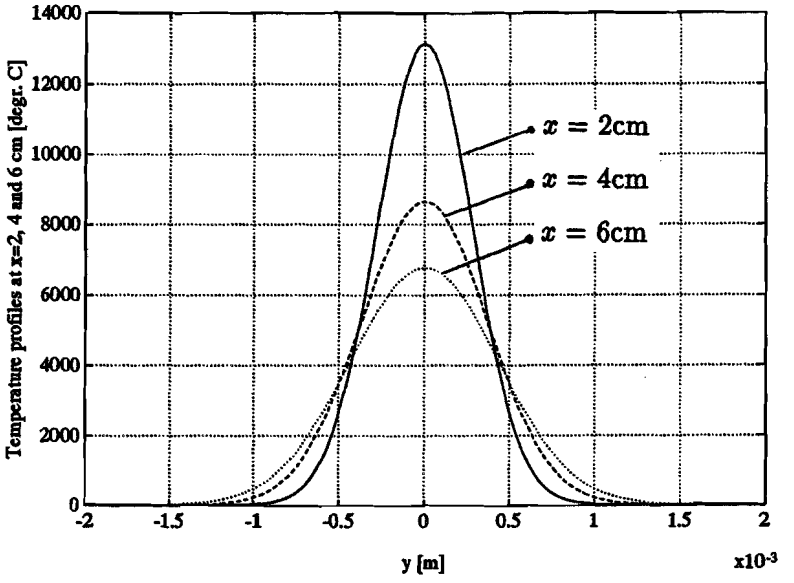

Figure 3.5: Temperature profiles at constant x

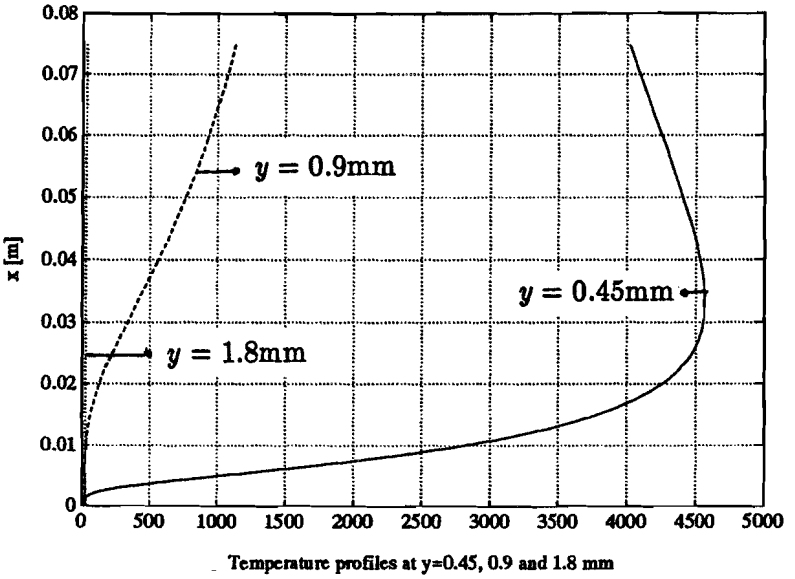

Figure 3.6: Temperature profiles at constant y

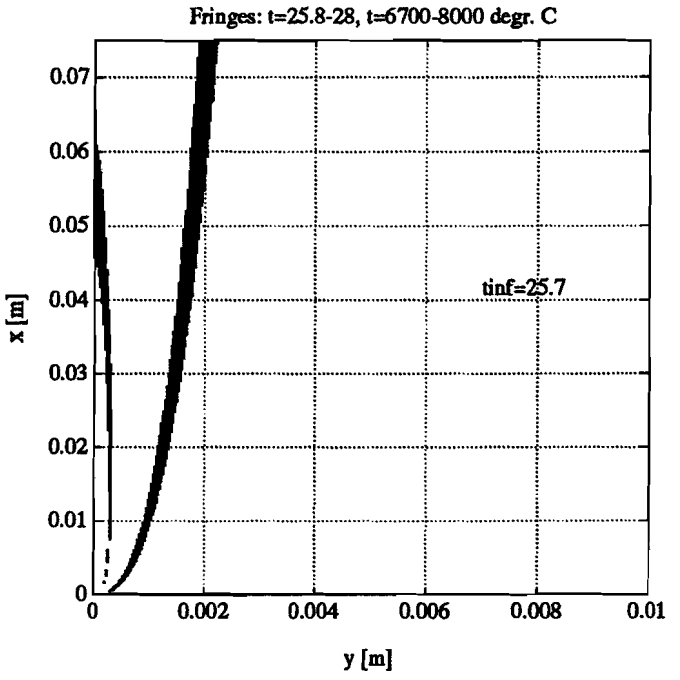

Figure 3.7: Calculated temperature fringes

From the inviscid solution it was found that the flow was much less stable for asymmetric disturbances then it was for symmetric ones. Also the dependence of the limit, the asymptote at high Grashof numbers, on the Prandtl number was calculated, see figure 3.9 (in the figure: $\beta \propto \omega_2 G^{1/3}$, with $G = 2\sqrt{2}(Gr_x)^{1/4}$).

Coupled and uncoupled solutions are given in figure 3.10 for $Pr = 0.7$. It is shown that the coupling term is important at low G but that its effect decreases as the Grashof number is increased. At extremely low values of G the boundary layer simplifications are no longer applicable. In figure 3.10 constant physical frequency lines are shown for a certain heat input ($Q = 56.3$ W/m) as they are convected by the base flow. At low frequency, the path enters deeply into the unstable region as G increases and these disturbances are strongly amplified. At sufficiently high frequency (in the figure: f>15 Hz) disturbances are always damped. In experiments, done by Pera and Gebhart [30] it was found that disturbances with frequencies higher than about 12 Hz were not detected downstream, disturbances of lower frequencies gave amplification. Total disruption of the flow happened at a shorter distance of the source with decreasing disturbance frequency. Thus experiments are in good agreement with the presented solutions.

3.4 Turbulent plumes

A general employed analysis of fully developed turbulent plumes is to consider integral conservation of mass, momentum and energy. Experimental information is used to model the entrainment of the ambient fluid into the flow. An important approximation is that the mean inflow in horizontal direction at the edge of the plume, i.e. where the vertical velocity is

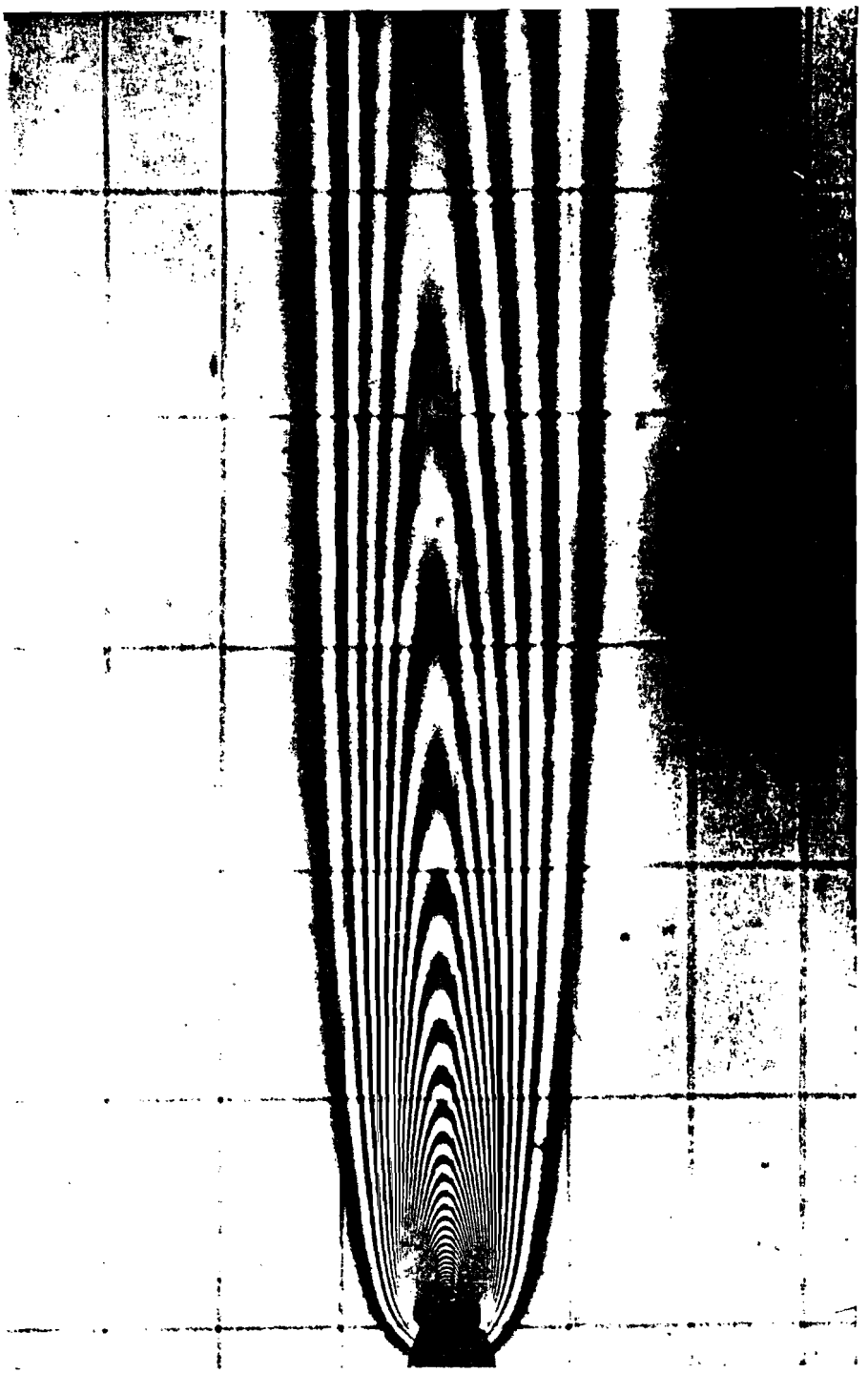

Figure 3.8: Interferogram (4.4° C per fringe, horizontal and vertical spacing of grid: $\frac{1}{2}$ and $\frac{1}{4}$ inch respectively).

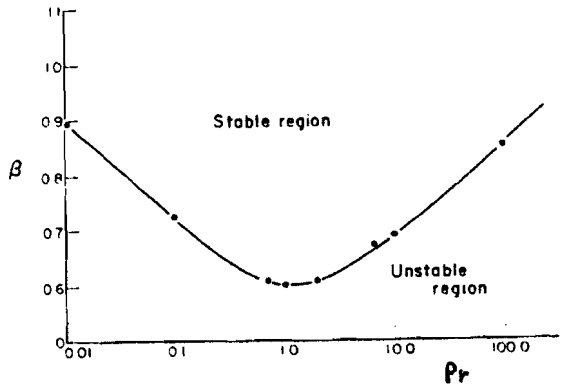

Figure 3.9: Effect of Prandtl number on stability. Inviscid and uncoupled case. Asymmetric disturbances

decreased to zero, is linear proportional to the local mean vertical velocity in the plume. According to this model the inflow velocity at the edge of the boundary layer is equal to αU, where α is the experimental determined constant of proportionallity, called the entrainment coefficient. Furthermore a top-hat profile is considered for both the temperature and the vertical velocity profile at some height x.

Employing these assumptions, the equations of conservation of mass, momentum and energy read:

$$\alpha U = \frac{d}{dx}(UR) \tag{3.27}$$

$$g\beta\Delta T R = \frac{d}{dx}\left(RU^2\right) \tag{3.28}$$

and

$$\Delta T R U = C \tag{3.29}$$

where C is a constant and R is the halfwidth of the plume at height x, and is assumed to be linear $R = cx$, where c gives the rate of spread. Trying a solution of the form $U \propto x^a$ and $\Delta T \propto x^b$ where a and b are constants, gives $a = 0$ and $b = -1$. This implies that U is not a function of x and that the temperature difference varies as $1/x$. From experiments it is known that α takes a value of approximately $\alpha \approx 0.08$. The equation for the conservation of mass shows that $c = \alpha$ and the solution for U and ΔT at given x is determined when these values are known at some height x.

Rouse, Yih and Humphreys [34] obtained experimentally a solution for the velocity and temperature profiles which they presented as:

$$u = 1.8\left(\frac{Q}{\rho_0}\right)^{\frac{1}{3}} e^{\left(-32y^2/x^2\right)} \tag{3.30}$$

and

$$\Delta T = \frac{2.6}{g\beta}\left(\frac{Q}{\rho_0}\right)^{\frac{2}{3}} \frac{1}{x} e^{\left(-41y^2/x^2\right)} \tag{3.31}$$

These are Gaussian distributions that give a similar behaviour as the solutions obtained above for the quantities at the centerline of the plume.

With the given solutions for turbulent plumes it can be stated that the Reynolds number, defined in the midplane, varies linear with x whereas in the laminar case, according to equation 3.24, it varies with $x^{6/5}$. The midplane Grashof number varies with x^2 in the turbulent case and with $x^{12/5}$ in the laminar situation.

3.5 Transition, uniqueness

Bill and Gebhart [2] determined the begin and end of transition of a plane plume in air by visual means, using an interferometer. Critical Gr-numbers were obtained by measuring the distance from the line source and the local temperatures at these points. The beginning of transition was found to be at about $Gr_x = 6.4 \cdot 10^6$. Large wave-like temperature disturbances were seen to have become very large at this height. The end of transition was also visually determined by noting the location in x at which a thickening of the mean flow boundary layer occurred without relaminarization at later times. This was observed to happen at approximately $Gr_x = 2.95 \cdot 10^7$. After the complete disruption of the boundary layer the flow begins to adjust to turbulent parameters, and the laminar centerline temperature is no longer achieved.

An important effect occuring in laminar natural convection flows that has to be taken into account is the non-uniqueness as reported by Gollub and Benson [15]. They observed several different flows to be stable for a given geometry, Grashof number and Prandtl number in Rayleigh-Bénard convection. This effect probably can influence the route to fully developed turbulence dramatically.

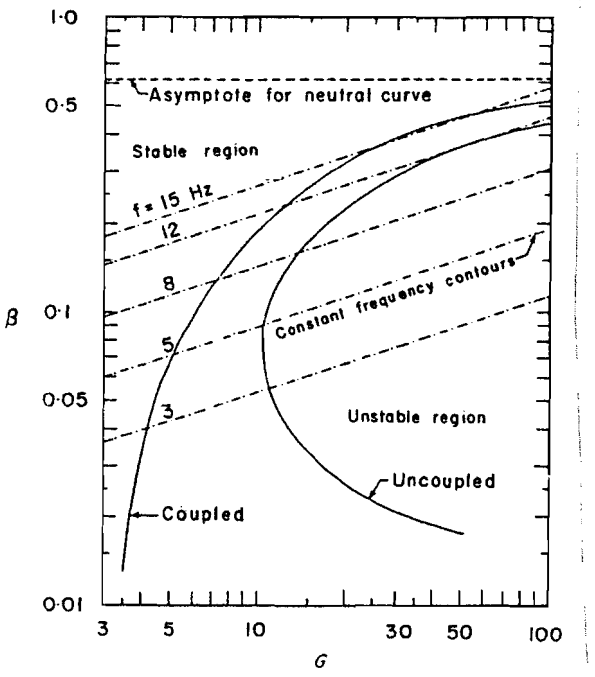

Figure 3.10: Computed neutral stability curves for asymmetric disturbances, $Pr = 0.7$

Chapter 4

Large eddy simulation

4.1 Numerical simulation of turbulent flows

Mostly, the natural convection flows of interest are in the transitional or turbulent regime. The important variables in such flows contain a spectrum of time and length scales from very small values to large integral ones. This range grows on the small scales side with the rate of forcing of the flow, indicated by the Grashof number. These scales are referred to as the Kolmogorov [20] microscales of time (τ) and length (η) and are given by:

$$\tau \equiv \left(\frac{\nu}{\epsilon}\right)^{1/2} \tag{4.1}$$

$$\eta \equiv \left(\frac{\nu^3}{\epsilon}\right)^{1/4} \tag{4.2}$$

in which ϵ is the dissipation rate per unit mass. The amount of kinetic energy per unit mass in the large scale turbulence is proportional to U^2, with U the characteristic velocity of these large scales with characteristic length L. In the inviscid limit the energy supply to the small scales is thus of the order $U^2 \cdot U/L$. This energy is dissipated at a rate ϵ which should be equal to the supply rate. Hence:

$$\epsilon \sim \frac{U^3}{L} \tag{4.3}$$

Since a turbulent flow is a solution of the Navier-Stokes equations we like to solve these equations up to the smallest scales of motion. If we take a three dimensional numerical grid we can approximate the equations for example with finite differences. The grid has to be three dimensional because the dynamics of turbulence is essential three dimensional, e.g. vortex stretching. Using a computer we can solve the resulting system of algebraic equations for each time step. By this means all important variables like velocity, temperature and pressure can be calculated all over the three dimensional field. Such rich information of a turbulent flow is very hard to get experimentally in a laboratory setup. A simulation like the one described in this section is called a direct simulation.

Because we want to solve the full turbulent structure with sufficient accuracy we can derive from the Kolmogorov relations for the smallest scales that the number of gridpoints has to satisfy:

$$N_g \sim \left(\frac{L}{\eta}\right)^3 \sim \left(\frac{UL}{\nu}\right)^{9/4} = Re^{9/4} \tag{4.4}$$

and the number of time steps:

$$N_t \sim \frac{L}{\tau U} \sim \left(\frac{UL}{\nu}\right)^{1/2} = Re^{1/2} \tag{4.5}$$

The total work will thus be proportional to $Re^{\frac{11}{4}}$ when the initial state of the turbulence is known. Even modern supercomputers do not have the capacity in the sense of both memory and speed to solve common turbulent problems of practical importance.

4.2 Reynolds decomposition

There are two procedures to reduce the computational work. The first one is the possibility to average each variable with respect to time. Another approach is to average the variables with respect to space. This spatial averaging procedure is the base of large eddy simulation and will be discussed in the next paragraph that is dealing with this subject.

The first procedure is usually referred to as the Reynolds decomposition and it splits a variable f into a mean part $\overline{f}$ and a fluctuating part f':

$$f(x_i,t) = \overline{f}(x_i) + f'(x_i,t) \tag{4.6}$$

$$\overline{f}(x_i) = \lim_{t^* \to \infty} \frac{1}{t^*} \int_{-\frac{t^*}{2}}^{\frac{t^*}{2}} f(x_i, t+\tau) d\tau \tag{4.7}$$

Applying this procedure to the variables in the Navier-Stokes equations and averaging the result we get the equations of motion for the averaged flow. Because of non-linearity terms like $\frac{\partial \overline{u_i' u_j'}}{\partial x_j}$ and $\frac{\partial \overline{u_i' T'}}{\partial x_j}$ appear. These terms express the influence of the smaller time scales variations on the average flow with respect to time and are called the Reynolds terms. Transport equations can be written down to determine these terms but new unknowns appear and so on. This closure problem is one of the central problems in turbulence theory. Several models have been developed to estimate the Reynolds terms, but there is no exact solution.

4.3 Theory of large eddy simulation

Another way of handling turbulence is large eddy simulation. Theory and applications of large eddy simulation are described in an extended review by Rogallo and Moin [33]. The basic ideas of this theory are presented in this section.

By applying large eddy simulation one makes use of a volume averaging or spatial filtering procedure. In general this procedure splits a variable f into a large scale component $\overline{f}$ that can be resolved and a small scale component f' by a convolution of f with a filter function G over the flow domain D:

$$f(x_i,t) = \overline{f}(x_i,t) + f'(x_i,t) \tag{4.8}$$

$$\overline{f}(x_i,t) = \int_D G(x_i - \xi_i) f(\xi_i,t) d\xi_i \tag{4.9}$$

or in wave number space:

$$\overline{f}(k_i,t) = G(k_i) f(k_i,t) \tag{4.10}$$

The filter function G has to satisfy the normalization condition, so that the filtered variable is not amplified or damped:

$$\int_D G(x_i - \xi_i) d\xi_i = 1 \tag{4.11}$$

It is also possible to average a quantity over a fixed volume cel. In contrast with the use of the filter operation this is not a running average. It's value will be piecewise constant over the cells. This method was used by Deardorff [8] and Schumann [37] and can be advantageous as will be explained in the following section.

Leonard [25] gave some examples of filters such as the top-hat or (continuous) volume average filter, the Gaussian filter and the Fourier cut-off filter[1]. The first two filters have identical second moments. The Fourier cut-off filter is a top-hat filter in wavenumber space. This filter thus passes low frequency modes and filters out the high frequency modes from a certain cut-off wave number. Since the Gaussian filter and the Fourier cut-off filter are extended on both sides to infinity they can be used when the flow domain is unbounded in space. When the flow is bounded the filtering procedure will not be symmetric anymore and the normalization condition is violated.

Integration by parts gives (according to [25]):

$$\overline{\frac{\partial f}{\partial x_i}} = \frac{\partial \overline{f}}{\partial x_i} \tag{4.12}$$

if G or f vanishes on the boundaries and it has to be noted that in general:

$$\overline{\overline{f}} \neq \overline{f} \qquad ; \qquad \overline{f'} \neq 0 \tag{4.13}$$

This can easily be seen by applying two times for instance a top-hat filter. The second condition follows from the first by filtering the decomposition 4.8.

If the characteristic filter width is taken proportional to the gridsize Δ the small scale component f' is a subgrid scale fluctuation. In this case full advantage is taken of computational effort. Filtering the non-dimensional Navier-Stokes equations in the Boussinesq formulation one gets:

$$\frac{\partial \overline{u}_i}{\partial x_i} = 0 \tag{4.14}$$

$$Sr\frac{\partial \overline{u}_i}{\partial t} + \frac{\partial}{\partial x_j}(\overline{u_i u_j}) = \frac{Gr}{Re^2}(\overline{T} - T_0)\delta_{i3} - \frac{\partial \overline{p}}{\partial x_i} + + \frac{1}{Re}\frac{\partial^2 \overline{u}_i}{\partial x_j^2} \tag{4.15}$$

$$Sr\frac{\partial \overline{T}}{\partial t} + \frac{\partial}{\partial x_j}(\overline{u_j T}) = \frac{1}{RePr}\frac{\partial^2 \overline{T}}{\partial x_j^2} \tag{4.16}$$

[1] The filters are governed by:

$$\text{Top-hat: } G_i^t = \begin{cases} 1/\Delta & -\Delta/2 < (x_i - \xi_i) < \Delta/2 \\ 0 & \text{else} \end{cases}$$

$$\text{Gaussian: } G_i^g = \sqrt{(6/\pi\Delta)}e^{-6(x_i-\xi_i)^2/\Delta^2}$$

$$\text{Fourier cut-off: } G_i^f = \frac{2\sin(\pi(x_i - \xi_i)/\Delta)}{\pi(x_i - \xi_i)}$$

in which:

$$\overline{u_i u_j} = \overline{(\overline{u}_i + u_i')(\overline{u}_j + u_j')} = \overline{\overline{u}_i \overline{u}_j} + \overline{u_i' \overline{u}_j} + \overline{\overline{u}_i u_j'} + \overline{u_i' u_j'} \equiv \overline{\overline{u}_i \overline{u}_j} + \eta_{ij} \tag{4.17}$$

Here the closure problem rises again. The terms containing subgrid scale variables have to be expressed in terms of the resolved variables. When the normal stresses are assumed to be isotropic they can be interpreted as a turbulent hydrostatic pressure. In this situation the normal stresses have no dynamic effect and therefore they are often added to the pressure term. Transporting the terms that contain subgrid scale quantities to the right hand side of the momentum equations results in:

$$Sr\frac{\partial \overline{u}_i}{\partial t} + \frac{\partial}{\partial x_j}(\overline{\overline{u}_i \overline{u}_j}) = \frac{Gr}{Re^2}(\overline{T} - T_0)\delta_{i3} - \frac{\partial}{\partial x_i}\left(\overline{p} + \frac{1}{3}\eta_{kk}\right) + \frac{\partial \tau_{ij}}{\partial x_j} + \frac{1}{Re}\frac{\partial^2 \overline{u}_i}{\partial x_j^2} \tag{4.18}$$

with

$$\tau_{ij} \equiv -\eta_{ij} + \frac{1}{3}\eta_{kk}\delta_{ij} \tag{4.19}$$

in which τ_{ij} describes the influence of the subgrid scales on the large scale effects and has to be modeled. Applying the same technique to the energy equation 4.16 results in:

$$Sr\frac{\partial \overline{T}}{\partial t} + \frac{\partial}{\partial x_j}(\overline{\overline{u}_j \overline{T}}) = \frac{\partial h_j}{\partial x_j} + \frac{1}{RePr}\frac{\partial^2 \overline{T}}{\partial x_j^2} \tag{4.20}$$

with

$$h_j \equiv -(\overline{\overline{u}_j T'} + \overline{u_j' \overline{T}} + \overline{u_j' T'}) \tag{4.21}$$

Here also a model has to be applied to determine h_j.

In large eddy simulations thus the large scale structure is explicitly calculated. The closure is only required for small scale effects. The Reynolds stresses on the other hand mainly depend on the large scale structure of the flow. Another advantage of large eddy simulation is the fact that the subgrid scale closure is relative easy because the micro scales have a more universal structure and can be described by relative simple theory. From simulations it is known that the simulated structures are rather insensible to details of the subgrid closure. With large eddy simulation it is possible to obtain detailed time dependent information of the flow. The computer effort required is reduced compared with direct numerical simulation.

4.4 Special treatment terms

As stated in the previous section the use of a Gaussian filter or Fourier cut-off filter in a bounded flow domain always gives rise to complications due to symmetry aspects and normalization of the filter. Also the validity of equation 4.12 is not guaranteed, e.g. for inhomogeneous directions. For this reason often a volume averaging method as applied by Schumann or a top-hat filtering technique are used. In the volume averaging method and in the case of application of the Fourier cut-off filter the filtered advection term for the large scales can be written as:

$$\frac{\partial}{\partial x_j}(\overline{\overline{u}_i \overline{u}_j}) = \frac{\partial}{\partial x_j}(\overline{u}_i \overline{u}_j) \tag{4.22}$$

$$\frac{\partial}{\partial x_j}(\overline{\overline{u}_j \overline{T}}) = \frac{\partial}{\partial x_j}(\overline{u}_j \overline{T}) \tag{4.23}$$

Frequently a finite difference method is used and the computed variables on the computational grid are regarded to as the resolved quantities $\overline{f}$. To obtain the resolved quantities the filtering procedure is not needed in this way. However a filter should be used to obtain the advection terms for the large scales as denoted in the left hand side of equations 4.22 and 4.23. Since $\overline{f}$ has become discrete an assumption has to be made about the continuous form of this variable. In most cases the identities 4.22 and 4.23 are used as an approximation or the discrepancy is said to be lumped in τ_{ij} to make life a little bit easier. Leonard [25] however, pointed out that these terms can be presented in the following way by using a Taylor series expansion for the resolved scales variables:

$$\frac{\partial}{\partial x_j}(\overline{\overline{u}_i\overline{u}_j}) \simeq \frac{\partial}{\partial x_j}\left(\overline{u}_i\overline{u}_j + \frac{\gamma_j}{2}\frac{\partial^2}{\partial x_k^2}(\overline{u}_i\overline{u}_j)\right) \tag{4.24}$$

This can also be done for the filtered large scale advection term for the temperature. Equation 4.24 makes use of γ_i the one-dimensional second moment of G which is equal to $\frac{\Delta^2}{12}$ in the case of the top-hat or Gaussian filter[2].

The mixed stress terms of resolvable scale components and subgrid scale components become zero in the volume averaging case because $\overline{f'}$ is then equal to zero. Hence:

$$\overline{\overline{u}_i u_j'} = \overline{u_i'\overline{u}_j} = \overline{\overline{u}_j T'} = \overline{u_j'\overline{T}} = 0 \tag{4.25}$$

Equation 4.25 holds also when a filter is used that is piecewise constant at values of 0 or 1 in wave space, since $\overline{f'} = G(1-G)f$ as can be derived[3] from equation 4.10. Using the Fourier cut-off filter thus allows the application of 4.25. When another filtering procedure is used these mixed terms (also called cross-terms) are neglected in most cases. Sometimes there's referenced to Clark et al. [4] who approximated the cross-terms, corrected for the normal stresses, with a Taylor series expansion as follows:

$$\overline{\overline{u}_i u_j'} + \overline{u_i'\overline{u}_j} \simeq -\frac{\Delta^2}{24}\left(\overline{u}_i\frac{\partial^2}{\partial x_j^2}\overline{u}_j + \overline{u}_j\frac{\partial^2}{\partial x_j^2}\overline{u}_i\right) \tag{4.26}$$

wherein the subgrid scale quantities disappear. The effect of the mixed terms is not very clear as is the effect of the approximations 4.22 and 4.23.

4.5 Subgrid scale models

In turbulent flows the viscous dissipation primarily takes place at the smallest scales of motion. The effects of these scales are modeled by applying a functional relation between the subgrid scale stresses τ_{ij} or fluxes h_{ij} and the resolved scale variables. The simplest and most commonly used models are those that are based on gradient diffusion:

$$\tau_{ij} = 2\nu_T\overline{S}_{ij} \tag{4.27}$$

[2]The one-dimensional second moment of G can be defined as:

$$\gamma_i = \int_{-\infty}^{+\infty} x_i^2 dx_i \int_{-\infty}^{+\infty} G(x_i, x_j, x_k) dx_j dx_k$$

[3]$\overline{f'} = \overline{f - \overline{f}} = \overline{f - Gf} = Gf - G^2 f = G(1-G)f$

$$h_{ij} = \nu_H \frac{\partial \overline{T}}{\partial x_j} \tag{4.28}$$

in which an eddy viscosity ν_T and an eddy diffusivity ν_H are defined. The resolved scale deformation rate tensor $\overline{S}_{ij}$ is given by:

$$\overline{S}_{ij} = \frac{1}{2}\left(\frac{\partial \overline{u}_i}{\partial x_j} + \frac{\partial \overline{u}_j}{\partial x_i}\right) \tag{4.29}$$

The eddy coefficients ν_H and ν_T depend on the local intensity of the turbulence. To determine the eddy viscosity a model proposed by Smagorinsky [40] in which the eddy viscosity is set proportional to the local large scale velocity gradient is widely used:

$$\nu_T = (C_s \Delta)^2 |\overline{S}| \tag{4.30}$$

Here C_s is a constant, the filter width Δ is a characteristic length scale of the smallest resolved eddies and $|\overline{S}| = \sqrt{\overline{S}_{ij}\overline{S}_{ij}}$. The value of C_s depends on the filter type and can be determined in various ways. The values of C_s that are used in large eddy simulations vary in the range $C_s = 0,07 - 0,24$, see Schmidt and Schumann [36].

Instead of the rate of deformation tensor S_{ij}, Kwak et al. [23] used the vorticity $\overline{\omega}_i = \epsilon_{ijk}\partial \overline{u}_k / \partial x_j$ as a measure for the intensity of the turbulence. The advantage of this approach is that there is no subgrid scale dissipation in irrotational flow areas.

Eidson [10] applied the Smagorinsky model to simulate natural convection flows. He modified the eddy viscosity ν_T by taking into account the buoyancy generated production of subgrid scale energy.

A more complicated model has been used by Nieuwstadt and Moeng [28] for natural convection flows in the planetary boundary layer. They define the turbulent viscosity in terms of the subgrid energy e:

$$\nu_T = C_\mu \Delta \sqrt{e} \tag{4.31}$$

for which a separate differential equation has to be solved. The subgrid energy e is defined as:

$$e = \frac{1}{2}\left(\overline{u_i^2} - \overline{u_i}^2\right) \tag{4.32}$$

It is found that in cases of forced convection the Smagorinsky model suffices best but that in natural convection flows a model of the form of 4.31 gives better results.

The subgrid heat fluxes are generally modeled analogous to the subgrid stresses. Most frequently the coefficients are therefore related to each other:

$$\nu_H = \frac{\nu_T}{Pr_T} \tag{4.33}$$

where Pr_T is the turbulent Prandtl number that varies between $Pr_T = \frac{1}{3} - \frac{1}{2}$, see Eidson [10].

All subgrid scale models discussed so far are based on isotropic and homogeneous turbulence and in these cases they suffice very well. Although in most practical situations where we are dealing with wall effects and spatial and temporal transition these features are not met. Therefore in recent years some important approaches to treat these cases have been developed.

An eddy viscosity model to simulate intermittent and non-homogeneous flows as in the transitional case was developed by Germano et al. [14]. In this model a Smagorinsky closure

was used in which the model coefficient was computed dynamically. It is based on an algebraic identity between the subgrid scale stresses at two different filtered levels and the resolved turbulent stresses. The obtained subgrid scale stresses vanish in laminar flow and at solid boundaries where a correct asymptotic behaviour of the turbulent boundary layer is predicted.

A totally different type of subgrid scale models, first proposed by Chollet and Lesieur [3], are developed based on spectral parametrization methods. They use the Eddy Damped Quasi-Normal Markovian (EDQNM) theory, in which the evolution of the energy spectrum is described. This model has no adjustable parameter and provides the possibility to backscatter subgrid scale energy to the mean flow. Initially it was only used for flows in unbounded spaces, using a box with periodical boundary conditions. Later on also bounded flow domains were simulated, e.g. the backward facing step by Silveira Neto et al. [39]. In this simulation the used subgrid scale model was generalized in physical space as proposed by Métais and Lesieur [26], and applied in a finite volume method.

Chapter 5

Numerical code

5.1 The numerically treated equations

The numerical code that was used is based on the non-dimensional Navier-Stokes equations. However, in free convection flows the Reynolds number is an induced quantity that can not be specified. This especially is the case in turbulent flows where the order of importance of all terms in the momentum equation is equal. Therefore the equations are non-dimensionalized in a somewhat different way compared to the method commonly used, described in chapter 2. A characteristic velocity scale can be obtained by balancing the convective and diffusion terms of the energy equation and assuming a characteristic length scale L. This gives:

$$u_i = \frac{\kappa}{L} u_i^* \tag{5.1}$$

$$x_i = L x_i^* \tag{5.2}$$

$$t = \frac{L^2}{\kappa} t^* \tag{5.3}$$

$$p = \frac{\kappa^2}{L^2} p^* \tag{5.4}$$

where the quantities denoted with the superscript * are non-dimensional. This superscript shall be omitted further on in this text.

By applying these relations the non-dimensional form of Boussinesq's formulation reads:

$$\frac{\partial u_i}{\partial x_i} = 0 \tag{5.5}$$

$$\frac{\partial u_i}{\partial t} + \frac{\partial}{\partial x_j}(u_i u_j) = Ra^* Pr (T - T_0)\delta_{i3} - \frac{\partial p}{\partial x_i} + \frac{\partial}{\partial x_j}\left(Pr \frac{\partial u_i}{\partial x_j}\right) \tag{5.6}$$

$$\frac{\partial T}{\partial t} + \frac{\partial}{\partial x_j}(u_j T) = \frac{\partial^2 T}{\partial x_j^2} \tag{5.7}$$

in which $Ra^* = Ra/(\Delta T)$, Ra being the Rayleigh number, defined as $Ra = GrPr$.

By introducing the spatial filter and the gradient diffusion concept for the subgrid quantities, one gets:

$$\frac{\partial \overline{u}_i}{\partial x_i} = 0 \tag{5.8}$$

$$\frac{\partial \overline{u}_i}{\partial t} + \frac{\partial}{\partial x_j}(\overline{\overline{u}_i \overline{u}_j}) = Ra^* Pr(\overline{T} - T_0)\delta_{i3} - \frac{\partial \pi}{\partial x_i} + \frac{\partial}{\partial x_j}\left((\nu_T + Pr)\frac{\partial \overline{u}_i}{\partial x_j}\right) \tag{5.9}$$

$$\frac{\partial \overline{T}}{\partial t} + \frac{\partial}{\partial x_j}(\overline{\overline{u}_j \overline{T}}) = \frac{\partial}{\partial x_j}\left((\nu_H + 1)\frac{\partial \overline{T}}{\partial x_j}\right) \tag{5.10}$$

The eddy diffusion constants are non-dimensionalized also and are derived from resolved dimensionless quantities. The quantities denoted with an overbar are filtered or resolved quantities. In the numerical procedure the filtering process is defined by the sampling of variables at the grid points. The length of the filter is of the order of the grid spacing.

5.2 Subgrid scale model

The turbulent viscosity is determined with the use of a subgrid energy. The subgrid energy is defined as $e = \frac{1}{2}(\overline{u_i^2} - \overline{u}_i^2)$. The expression for the turbulent viscosity then reads:

$$\nu_T = C_\mu \Delta \sqrt{e} \tag{5.11}$$

with a constant C_μ and a representative grid spacing Δ. The subgrid heat fluxes are related to the subgrid stresses by a turbulent Prandtl number of magnitude $Pr_T = \frac{1}{3}$. This gives:

$$\nu_H = \frac{\nu_T}{Pr_T} = 3\nu_T \tag{5.12}$$

Since the grid spacing is taken to be equidistant in this study, the definition of a representative grid distance Δ by the average of the spacing in all directions or by the enclosed volume is the same. The constant C_μ has a characteristic value of $C_\mu = 0.12$. This value was determined by Schmidt and Schumann [36] by assuming a local equilibrium of shear-production and dissipation and has proved to give good results.

To determine the eddy coefficients a differential equation for the subgrid energy is used. This equation is given in appendix D. All turbulent diffusion coefficients are determined from the previous time step. The subgrid energy equation is a convection-diffusion equation, containing source terms and a sink. For more details see appendix D.

5.3 Discretization and solution process

The method used for solving the governing equations was introduced by Harlow and Welch [17]. The equations are discretized on a staggered grid as depicted in figure 5.1 for the two dimensional case. All scalar variables are defined at the centre of each cell and the velocity components are defined at the cell faces. The use of the staggered grid permits coupling of the velocity and pressure solutions at adjacent grid points. This prevents the appearance of oscillatory solutions which is a manifestation of two separate pressure solutions associated with alternate grid points.

The spatial discretization scheme is based on central differences. The advection terms are treated by a central difference method proposed by Piacsek and Williams [31]. This scheme conserves energy and avoids nonlinear instability. The time integration is carried out by a leap-frog scheme. The leap-frog method is desirable because it has neutral numerical stability (it neither amplifies nor damps), see Deardorff [9]. To avoid time splitting of the solution a weak time filter (Asselin [1]) is applied after each time step.

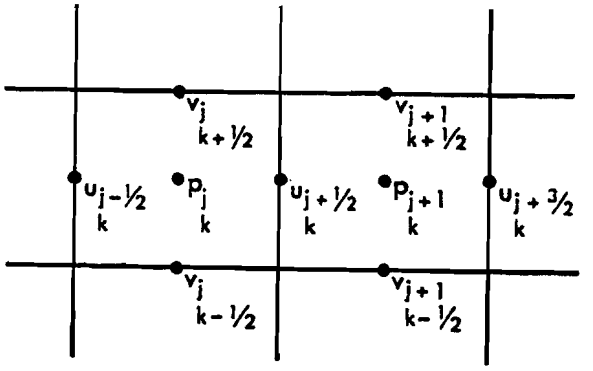

Figure 5.1: Staggered grid

The method consists of solving a Poisson equation for the pressure on the staggered grid at every time-step. The Poisson equation is obtained by taking the divergence of the momentum equation 5.9:

$$\frac{\partial^2 \pi}{\partial x_i^2} = \frac{\partial R_i}{\partial x_i} - \frac{\partial}{\partial t}\frac{\partial \overline{u}_i}{\partial x_i} \tag{5.13}$$

in which R_i contains the contributions of the non-linear, buoyancy and diffusion (resolved and subgrid) terms. With this equation the modified pressure π at time-step n is evaluated by taking the non-linear and buoyancy terms from time-step $(n-1)$ and the diffusion from step $(n-2)$. The instationary term is approximated by:

$$\frac{\partial}{\partial t}\frac{\partial \overline{u}_i}{\partial x_i}\bigg|_{n-1} \approx \frac{1}{2\Delta t}\left(\frac{\partial \overline{u}_i}{\partial x_i}\bigg|_{n} - \frac{\partial \overline{u}_i}{\partial x_i}\bigg|_{n-2}\right) \tag{5.14}$$

To force the solution to a divergence-free flow field the first term on the right-hand side is assumed to be zero to satisfy the continuity equation 5.8. The tiny value of divergence that existed at time-step $(n-2)$ is kept to guarantee that the divergence never grows beyond the value it can attain in one time-step through inaccuracies or roundoff errors in the solution of the Poisson equation (see Harlow and Welch [17] and Deardorff [9]). The result is the Poisson equation given by:

$$\frac{\partial^2 \pi}{\partial x_i^2}\bigg|_{n} \approx$$
$$\frac{\partial}{\partial x_i}\left(\frac{\overline{u}_i}{2\Delta t}\bigg|_{f(n-2)} - \frac{\partial}{\partial x_j}(\overline{u_i u_j})\bigg|_{n-1} + \frac{\partial}{\partial x_j}(\nu_T + Pr)\frac{\partial \overline{u}_i}{\partial x_j}\bigg|_{f(n-2)} + Ra^* Pr(\overline{T} - T_0)\delta_{i3}\bigg|_{n-1}\right) \tag{5.15}$$

Herein the term $(\overline{u_i u_j})$ is assumed to be equal to $(\overline{u}_i \overline{u}_j)$ as explained in the previous chapter. Equation 5.15 was solved using a standard computer package. The obtained pressure is used as an approximation for the pressure at time step n.

After having obtained a solution for the pressure the instationary term of the momentum equation 5.9 can be calculated and the time-stepping can be performed according to the

leap-frog scheme. After this the Asselin filter [1] is applied:

$$f_{f(n-1)} = 0.8 f_{n-1} + 0.1 f_n + 0.1 f_{f(n-2)} \tag{5.16}$$

The terms in equation 5.15 and 5.16 defined at time step $(n-2)$ are filtered terms according to this filter.

The maximum time-step is limited by a criterion given by Pourquié [32]. It was found by stability analysis in which only the combined step of advection and diffusion was treated. Pressure and source terms were not taken into account. A lower bound for the maximum admissible time-step was given by:

$$\Delta t \leq \min \left\{ \left(\left| \frac{\overline{u}_i}{\Delta x_i} \right| + 4(\nu_T + \nu_H) \frac{1}{\Delta x_i^2} \right)^{-1} \right\} \tag{5.17}$$

For the boundary conditions either periodic conditions or wall conditions can be adopted to prescribe the velocities, temperatures and pressures or their derivatives on the boundaries of the flow domain. Conditions for quantities that are not defined on the boundaries are determined with linear interpolation between a virtual grid point outside the domain and a grid point in the flow domain. Also a heatflux can be adopted on the boundaries. The code converts a heatflux condition to a fixed temperature condition at each time-step.

The initial conditions are usually imposed by prescribing a realistic mean temperature and velocity field. Upon these initial fields perturbations are superposed to trigger the turbulent characteristics of the flow.

In table 5.1 the basic steps are given for the solution process at each time step as it is implemented in the time loop. All $(n-2)$ terms are filtered terms. Here only the velocity is taken into account, treatment of the temperature and subgrid energy are trivial.

no.	Basic step	Comment
1	Set boundary conditions	-
2	Determine eddy diffusion coefficients	Eq. 5.11, 5.12
3	$A = \frac{\overline{u}_i}{2\Delta t}\Big\|_{f(n-2)} - \frac{\partial}{\partial x_j}(\overline{u_i u_j})\Big\|_{n-1} + \frac{\partial}{\partial x_j}(\nu_T + Pr)\frac{\partial \overline{u}_i}{\partial x_j}\Big\|_{f(n-2)} + + Ra^* Pr(\overline{T} - T_0)\delta_{i3}\Big\|_{n-1}$	Eq. 5.15
4	$B = \frac{\partial}{\partial x_i} A$	Eq. 5.15
5	Solve the Poisson equation	Eq. 5.15
6	$\frac{\partial \overline{u}_i}{\partial t}\Big\|_n = A - \frac{\overline{u}_i}{2\Delta t}\Big\|_{f(n-2)} - \frac{\partial \pi}{\partial x_i}\Big\|_n$	Eq. 5.9
7	$\overline{u}_i\|_n = \overline{u}_i\|_{f(n-2)} + 2\Delta t \frac{\partial \overline{u}_i}{\partial t}\Big\|_n$	Leap-frog scheme
8	$\overline{u}_i\|_{f(n-1)} = 0.8\overline{u}_i\|_{n-1} + 0.1\overline{u}_i\|_n + 0.1\overline{u}_i\|_{f(n-2)}$	Eq. 5.16
9	Determine the time step Δt	Eq. 5.17

Table 5.1: Basic solution process for the velocity at time step n

Chapter 6

Preliminary results

6.1 Plane plumes in large aspect ratio domains

As in all simulated cases the flow domain in the plane plume calculations consisted of a rectangular box (see figure 6.1) that was discretized by an equidistant grid in all directions. The box contained a finite heating strip situated at the lower boundary over the full j-direction

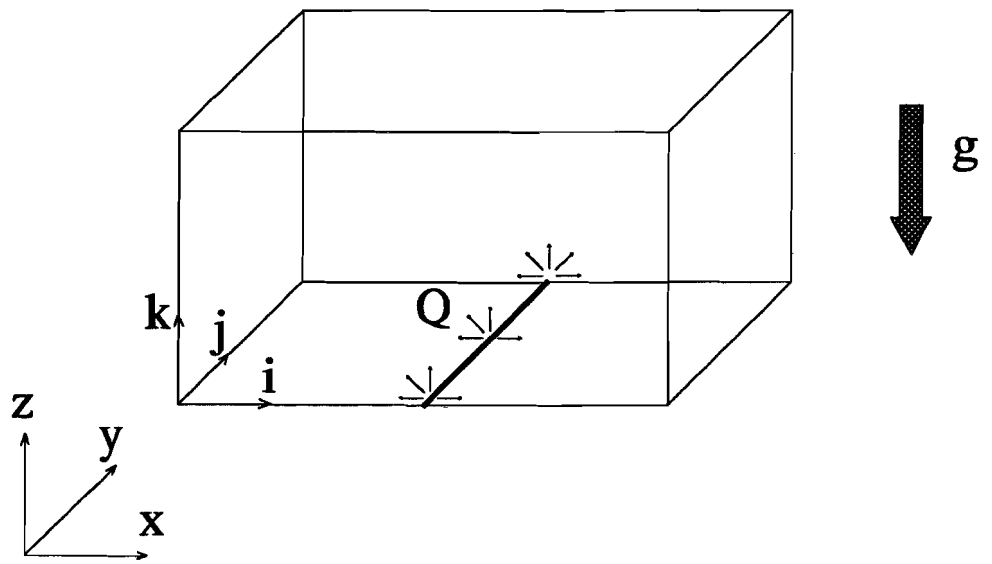

Figure 6.1: Considered flow configuration

at position i that is nearest to $i_{max}/2$ (which gives not always perfect symmetric solutions for i_{max} even). Several combinations of box sizes, boundary conditions and rate of forcing

of the flow by the heat source were tried out in order to get some feeling for the outcome of the calculations. This information together with insight in physical reality should lead to an optimal design of an experiment both in the numerical and physical sense that can be matched.

In order to observe some transitional behaviour of the flow most flow domains are taken large in the i-direction, i.e. the direction perpendicular to the line heat source in the horizontal plane. Also some calculations were performed with more cubical shaped boxes.

The first calculations were performed on a $80 \times 8 \times 8$-grid[1]. Some flow quantities are given in table 6.1 and some important pictures of subgid energy and velocity field can be seen in figures 6.2, 6.3 and 6.4.

Ra^*	ΔT	Gr	N	t_{end}	U_{max}	$\sqrt{e_{max}}$	$U_{max}/\sqrt{g\beta\Delta TL}$
10^4	98	$9.8 \cdot 10^5$	2000	0.31	152	74	0.154
10^5	92	$9.2 \cdot 10^6$	4500	0.30	384	196	0.127
10^6	87	$8.7 \cdot 10^7$	4500	0.127	847	404	0.091
10^7	86	$8.6 \cdot 10^8$	4500	0.0596	1848	845	0.063
10^8	84	$8.4 \cdot 10^9$	50000	0.3015	4077	1840	0.044

Table 6.1: Results of calculations on a $80 \times 8 \times 8$*-grid*

The Prandtl number was set equal to $Pr = 1$ and the Grashof number (or the Rayleigh number which is the same in this case) was varied in five steps over the decades of the interval $Gr \approx 10^6 - 10^{10}$. In the table the number of time steps is denoted by N, t_{end} is the simulated time, U_{max} the maximum velocity and e_{max} the maximum subgrid energy. These quantities are all non-dimensional as described in the previous chapter. The last column shows the maximum velocity obtained by scaling with $\sqrt{g\beta\Delta TL}$. The boundary conditions were prescribed by adiabatic no slip walls at the top and bottom, periodic boundary conditions at the left, right, front and back, and a heat flux at the line source. In this case the box keeps warming up at a certain rate prescribed by the heat flux and dimensions of the domain. The driving buoyant force remains constant so the velocity field develops to a stationary situation. The obtained solution is of limited physical relevance since the fluid properties are kept constant while the temperature increases. As initial condition a no-flow condition was applied, slightly perturbed with a random velocity field[2]. When the heat flux was set to zero this velocity field vanished after some time.

Most flow calculations were carried out over 4500 time steps, which means that the actual passed time got shorter with increasing Grashof number. This because of the dependence of the size of the time step on the stability of the calculation. Nevertheless the main features of a developed flow could be observed in all cases.

The flow starts with the forming of a two-dimensional mushroom shaped dipole vortex that travels from the heat source to the top wall where it collides. At this moment the sole monopoles see their own image (these are secondary vortices in the wall, caused by no slip)

[1]The characteristic length L and temperature difference ΔT scales in the Grashof and Rayleigh number are constantly based on height of the box (that is always set to $L = 1$) and maximum temperature difference within the flow domain.

[2]The perturbing random velocity field is not divergence free but after one solution of the Poisson equation a divergence free velocity field remains.

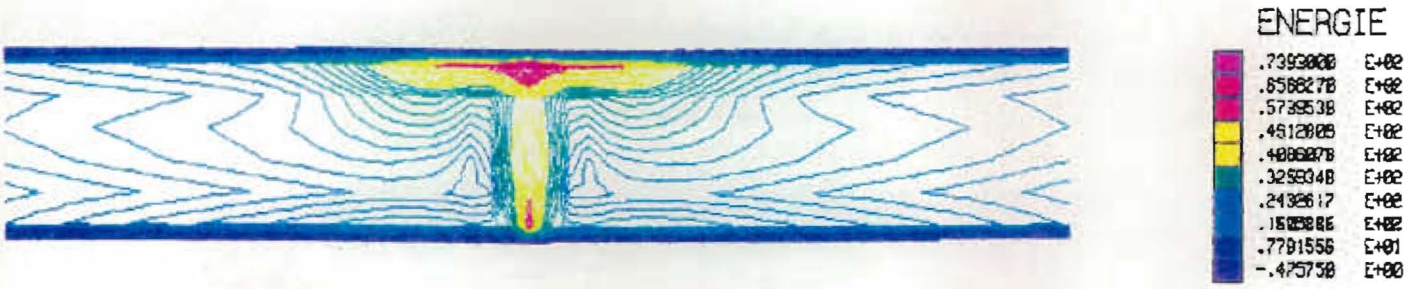

Figure 6.2: Subgrid energy field for $Gr = 9.8 \cdot 10^5$

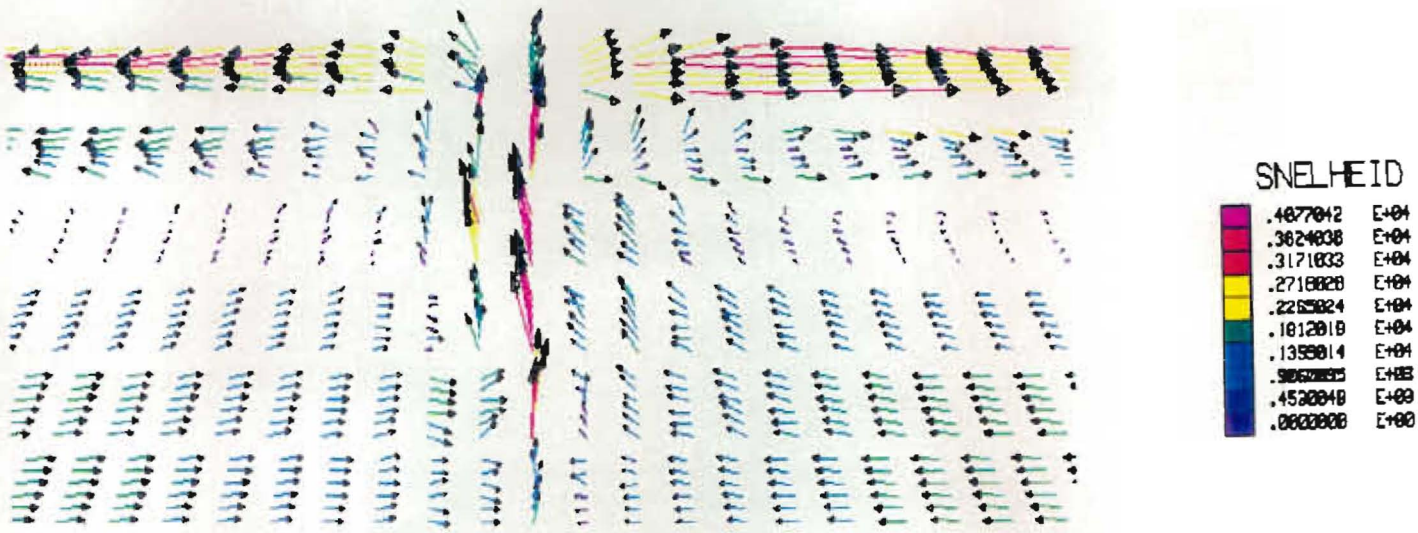

Figure 6.3: Velocity field in the center region for $Gr = 8.4 \cdot 10^9$

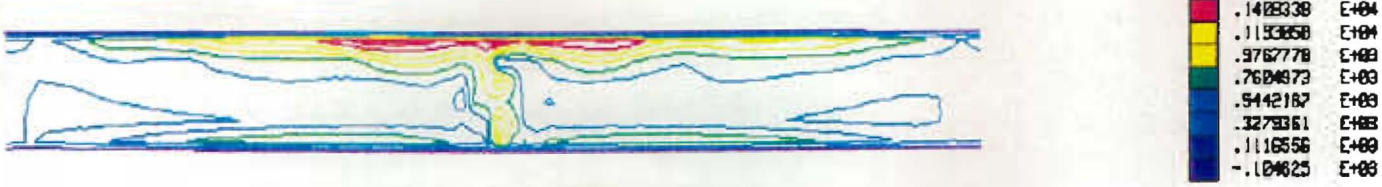

Figure 6.4: Subgrid energy field for $Gr = 8.4 \cdot 10^9$

in the top wall and form with these images new dipoles moving away from each other. In this way the vortices start to travel round in their own half of the flow domain undergoing diffusion of impuls and driving of the heat source. After some time the main structure of the flow consists of two big vortices filling the entire flow domain, with their axis parallel to the heat source. This structure remains the same with increasing Grashof number but becomes turbulent in the rising zone above the source and in the spreading area at the top of the flow domain.

The observed maximum velocities, non-dimensionalized by $U = \sqrt{g\beta\Delta TL}$, varied from 0.154 to 0.044 at the lowest and highest Grashof number respectively. This maximum appears halfway the height of the box at low Grashof numbers (laminar case), moves up with increasing Grashof number and goes down again as the flow is getting more turbulent. A relative small amount of subgrid energy is produced in the neighbourhood of the heat source (fig. 6.2). This subgrid energy is convected with the plume to the top where most of the subgrid energy is produced caused by the collision of the plume with the top wall. This energy is dissipated as it is convected away.

The transition to turbulence can be observed in the structure of the subgrid energy field, the evolution to three-dimensional flow and the intantaneous deviation of symmetry in the flow field. The first bifurcation is best to see in the blob structure of the spatial subgrid energy distribution, see figure 6.4. These blobs travel from the line source where they are generated towards the top at $Gr = 9.2 \cdot 10^6$. At higher Grashof numbers a velocity component parallel to the heat source is observed if looked at the flow field at a fixed time, see figure 6.3. The dynamics is then governed by thermals, high speed areas where the flow breaks through. At some distance from the plume the two dimensional field is redeveloped and especially in the regions of the big vortices where the fluid is supplied to the plume again the flow is two-dimensional, even at the highest simulated Grashof number. This flow is still instationary. It has to be notified that there is almost no transport across the left and right boundaries.

In figures 6.5 and 6.6 and in appendix C the vertical velocity in some point $w(50, 6, 6, t_i)$ is plotted as function of time. Also the frequency spectrum of this velocity component is given in these figures.

At low Grashof number a stationary flow arises after starting effects have vanished. With the increase of the forcing a traveling wave shows up in the registered signal. The amplitude and the frequency of this wave grows with the forcing and the wave becomes unstable. Some more details of the time series at the highest forcing can be found in appendix B. From the figures in appendix C it follows also that the starting behaviour of the flow is essentially similar and that the bifurcation can not be seen at this moment. The flow develops faster with higher forcing but the time steps become smaller. From the calculations presented however it can be concluded that the number of time steps needed to calculate a developed flow stays approximately constant.

At the highest Grashof number there are many frequency components. Very high frequencies that are associated with small length scales are probably not occuring due to the coarseness of the numerical grid. In this way a spatial filter always works as a frequency filter too.

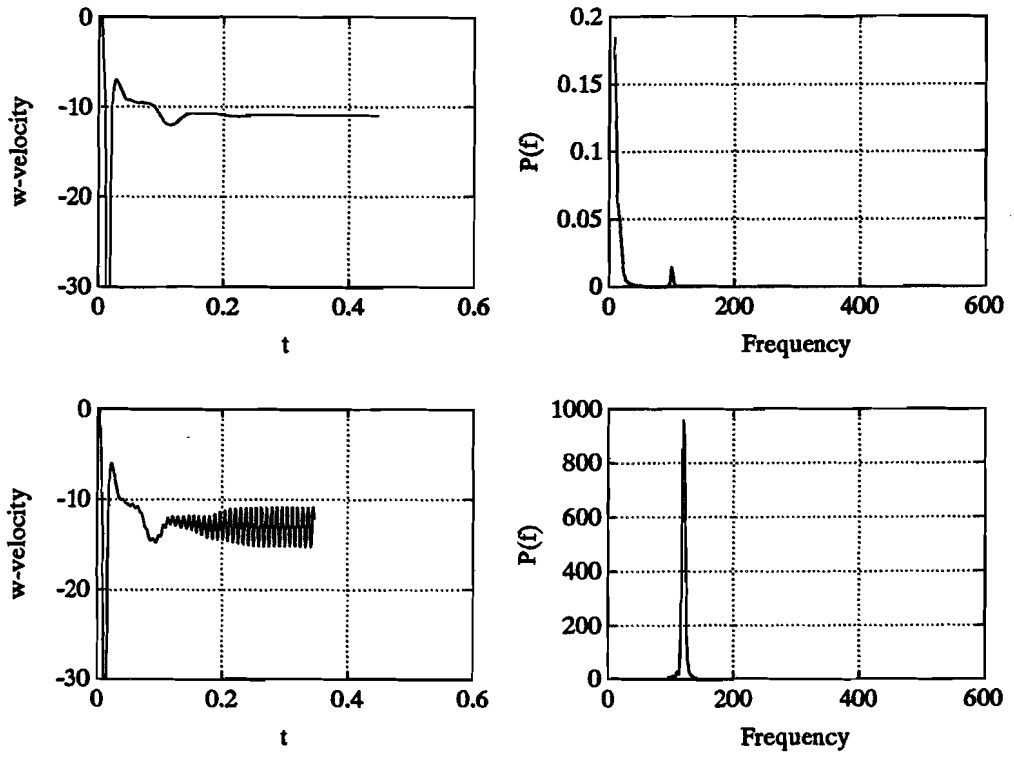

Figure 6.5: $w(50,6,6,t_i)$ *and* $P(50,6,6,f)$ *at* $Gr = 4.8 \cdot 10^6$ *and* $Gr = 7.5 \cdot 10^6$

6.2 Other plane plume simulations

Calculations were also performed for a more cubical flow domain. Here an equidistant grid of $14 \times 8 \times 14$ nodes was used. The applied boundary conditions were the same as in the former case except for the top wall that was kept on the initial temperature. At $Gr = 4.9 \cdot 10^6$ a stationary oscillating flow arises. This flow consists of two big counter-rotating vortices traveling from left to right through the flow domain, see figure 6.9. While doing this one vortex grows relatively to the other because it receives more buoyant energy due to its location with respect to the heat source. At the same time the smaller vortex is pushed up to the top and a main flow develops going from left to right over the first vortex and under the second flowing out of the domain. At this moment there is almost no flow in the neighbourhood of the heat source and a relatively hot region is created. A thermal develops and breaks through the main stream to reorganize the flow in two big vortices which start to move again. From this point the whole process starts all over again.

As can be seen in figure 6.10 a period doubling has appeared, but the reason of the main differences between the alternating periods could not be detected.

It is also shown that the flow is still fully two-dimensional (pay attention to the scales). This is in contradiction to the general case wherein the second bifurcation usually exploits a new dimension. The two distinguished orbits in the phase portrait also have some structure as can be seen in figure 6.11, that is a blown up detail of figure 6.10.

It is not clear if these effects are due to the fact that starting effects are possibly not

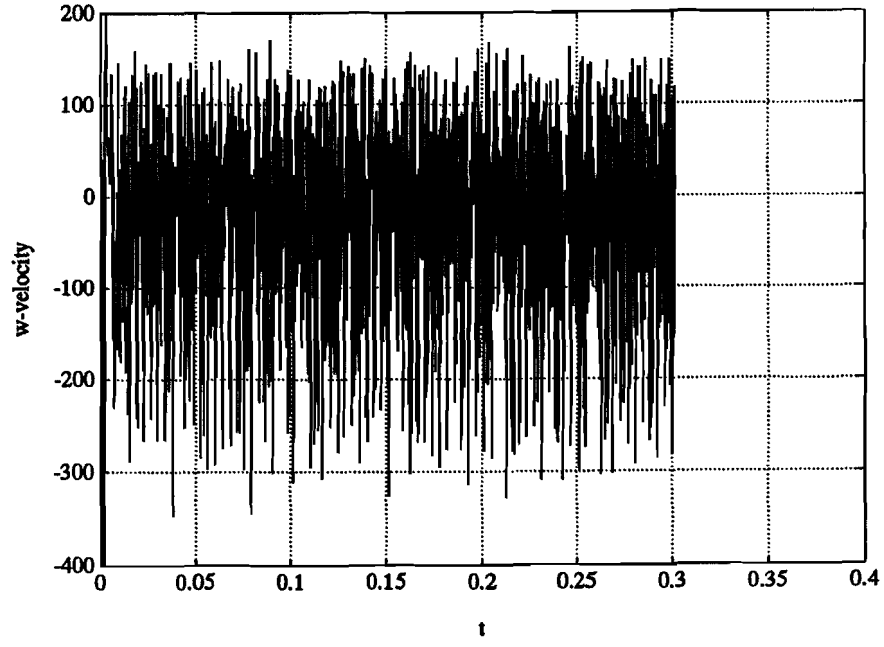

Figure 6.6: $w(50, 6, 6, t_i)$ *at* $Gr = 8.4 \cdot 10^9$

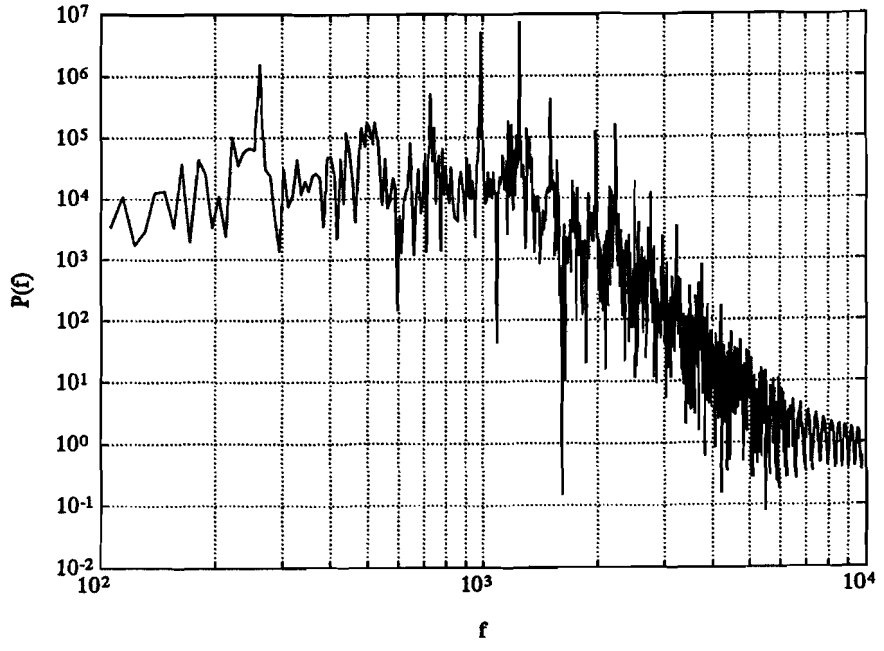

Figure 6.7: $P(50, 6, 6, f)$ *at* $Gr = 8.4 \cdot 10^9$, *logarithmic plot*

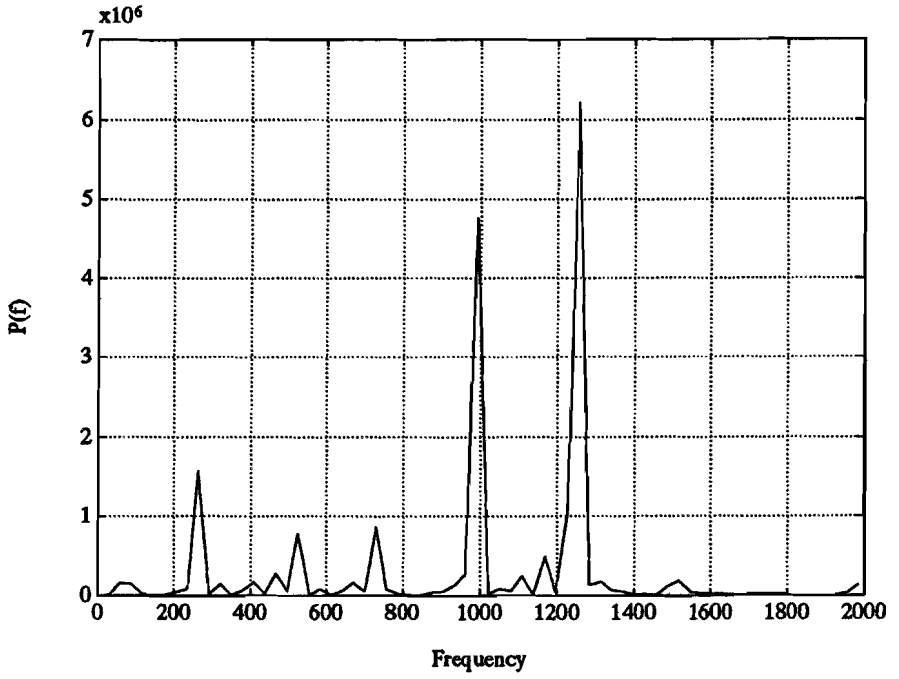

Figure 6.8: $P(50, 6, 6, f)$ *at* $Gr = 8.4 \cdot 10^9$, *linear plot*

damped out yet. After the start all variables were getting periodic (ten periods were calculated) with constant mean (as function of time), but the mean temperature was still increasing and only in the end it approximated a constant value.

Simulations of flows at high Grashof numbers in a more or less cubical box resulted in a local turbulent flow that still formed one coherent vortex, filling almost the entire domain, see figure 6.12. The departure of the plume was not straight up but oriented to the left or right. Because of the existence of large co-rotating vortices in the periodic direction, areas of high shear and whirling structures appear.

Also in the case of application of adiabatic walls on the left and right side of the heat source one vortical structure develops (see also figure 6.12. In this case it is observed that a high temperature region sustains in the right upper corner while the flow is rotating counter-clockwise. Probably this is a rudimentary relic of the first thermal that diffuses only slowly and is located in an area where the advection process is not very effective either. In this case the region of high subgrid energy is moved to the left side wall.

The formation of a single coherent vortex instead of two in a cubical flow domain could be due to the action of inertia forces. These forces cause the flow to be as less curved as possible. Also the velocity gradients are low in the one-vortex case. From a viewpoint of minimal viscous dissipation the formation of a single vortex is more advantageous.

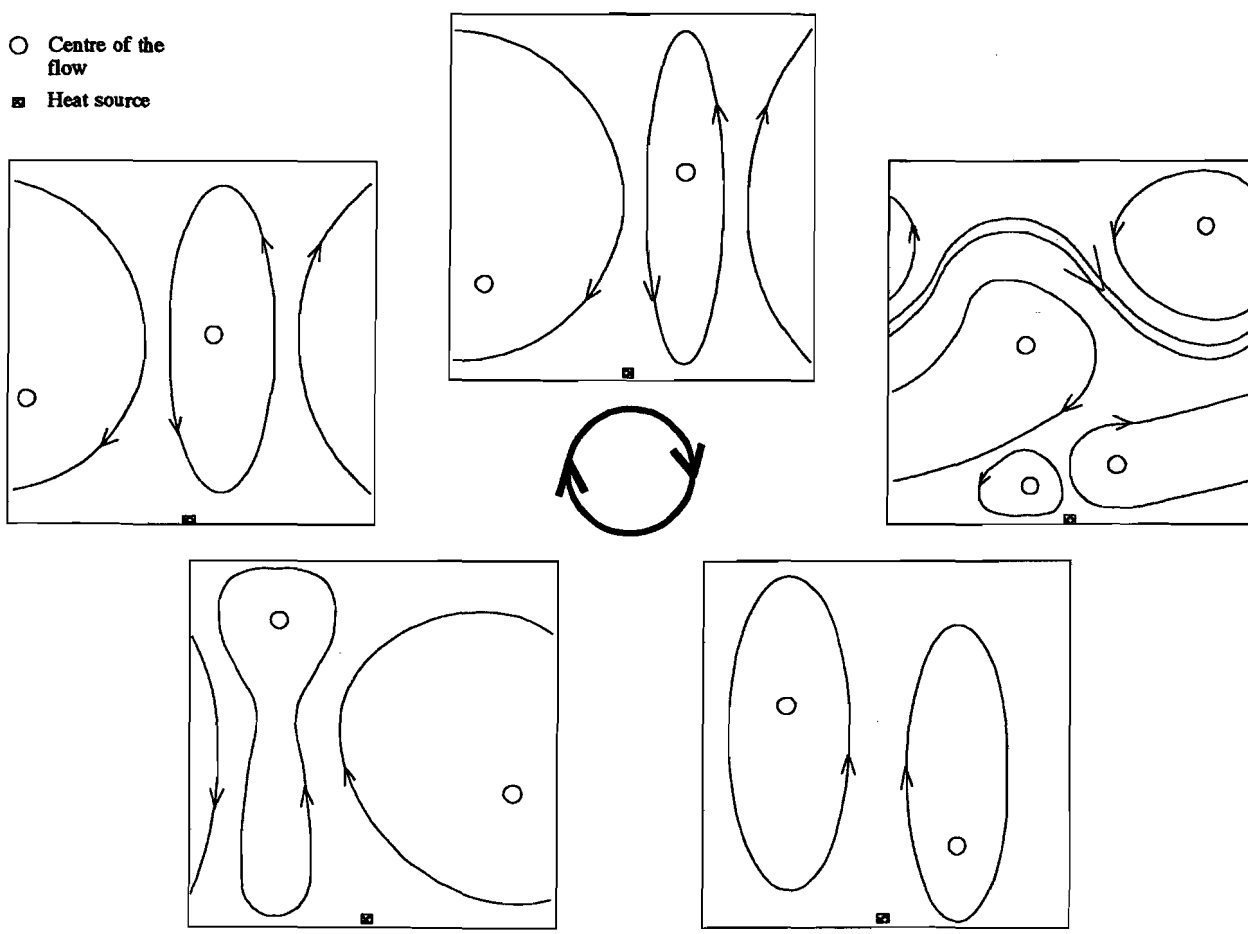

Figure 6.9: Topology of the obtained flow

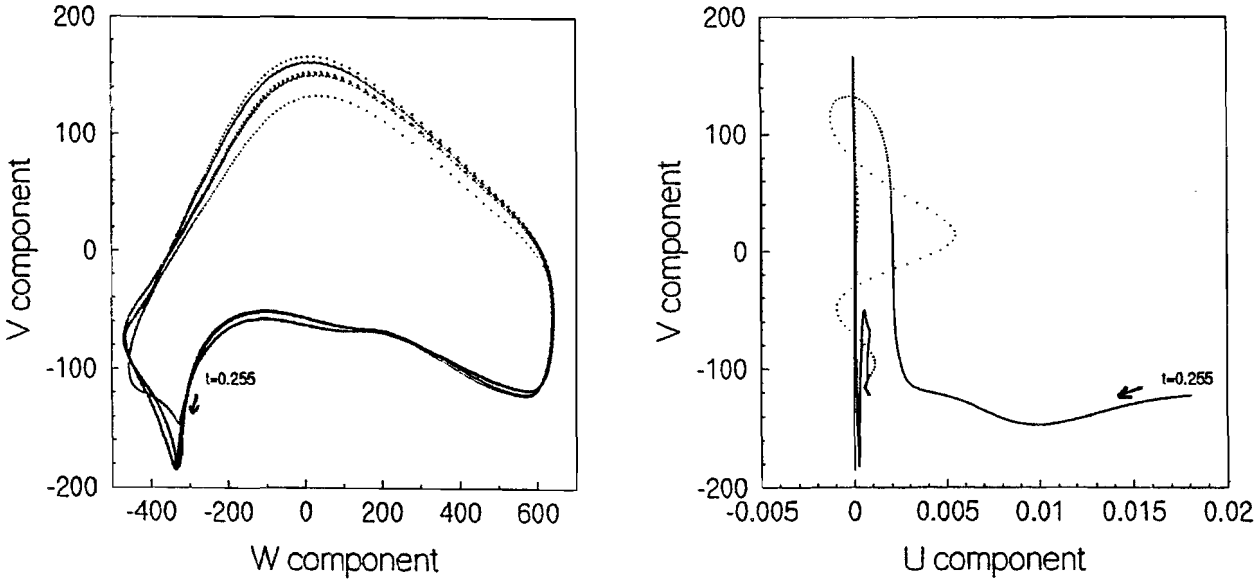

Figure 6.10: Phase portrait presentation at $Gr = 4.9 \cdot 10^6$

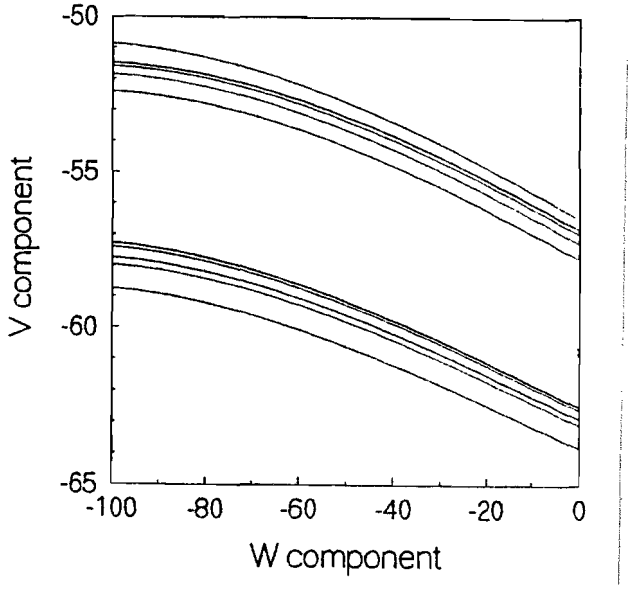

Figure 6.11: Detail of the phase portrait at $Gr = 4.9 \cdot 10^6$

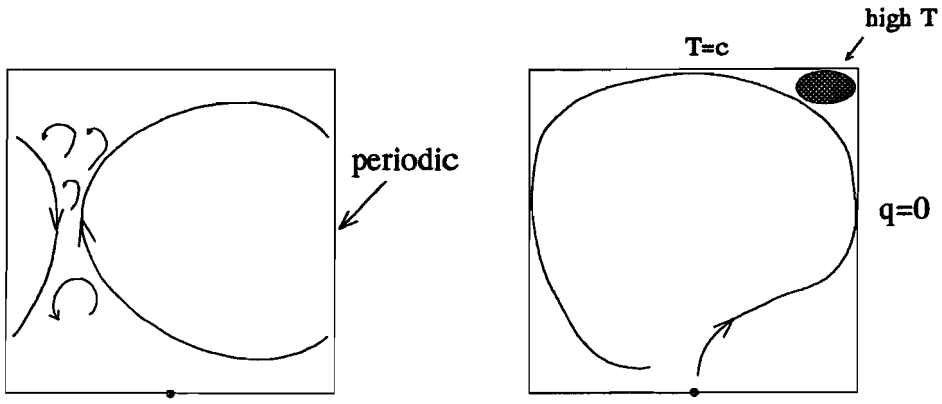

Figure 6.12: Formation of one coherent vortex, applying (left) periodic boundary conditions and (right) no-slip walls

6.3 Presence of a supercritical Hopf bifurcation

In the a previous section it has been showed that the first instationary motions of the flow induced by a thermal line source in some configuration consists of a single frequency oscillating motion. The amplitude increases with the forcing of the flow. The start of a single frequency, the first spike in the frequency spectrum, is the first step to a broad band spectrum that is characteristic for fully developed turbulence.

It is possible to determine the stability of the flow by perturbing it with very small disturbances. The stability against very small disturbances is denoted as the linear stability of the flow. In the numerical code these disturbances were introduced in the initial condition of the velocity field and it was observed that above some critical Grashof number, Gr_{cr}, the flow is not linearly stable. We can also consider analytically a basic stationary flow that is perturbed and therefore developing in time:

$$u_(x_i, x_j, x_k, t) = u_0(x_i, x_j, x_k) + u_1(x_i, x_j, x_k, t) \tag{6.1}$$

In this way u_1 must be determined from the full equations of motion. According to Landau and Lifshitz [24] the general solution can be represented as a sum of particular solutions in which u_1 depends on time as $e^{-i\omega t}$. By solving the equations of motion with the appropriate boundary conditions the frequencies ω are determined. If there are frequencies $\omega = \omega_1 + i\gamma_1$ whose imaginary parts are positive, $e^{-i\omega t}$ will increase indefinitely with time. For the flow to be stable it is necessary that the imaginary parts are all negative. The perturbations that arise will then decrease exponentially with time.

We now consider instationary flows at Grashof numbers slightly greater than Gr_{cr}. In this case there is a frequency ω_1 with a positive imaginary part γ_1. The function u_1 corresponding to this frequency is of the form:

$$u_1 = A(t) f(x_i, x_j, x_k) \tag{6.2}$$

where f is some complex function of the coordinates and the complex amplitude $A(t)$ is given by:

$$A(t) = Ce^{\gamma_1 t} e^{-i\omega_1 t} \tag{6.3}$$

This expression for $A(t)$ is only valid during a short interval of time after the perturbation of the basic flow. The factor $e^{\gamma_1 t}$ increases rapidly with time, whereas the method of determining u_1 from the full equations that leads to 6.2 and 6.3 is only valid when $|u_1|$ is small. The modulus $|A|$ of the amplitude of the flow does not increase unlimited but tends to a finite value. For Gr close to Gr_{cr} this finite value is small and can according to Landau and Lifshitz [24] be determined as follows.

For small values of t, when 6.3 is still valid the time derivative of the squared amplitude $|A|^2$ is given by $d|A|^2/dt = 2\gamma_1|A|^2$. This expression is the first term in an expansion in series of powers of A and A^*. As the modulus $|A|$ increases subsequent terms in this expansion must be taken into account. Since the third order terms contain the periodic factor and the fact that we are interested in the time average of $d|A|^2/dt$ we get, including the fourth order terms:

$$\frac{d|A|^2}{dt} = 2\gamma_1|A|^2 - \alpha|A|^4 \tag{6.4}$$

that is generally referred to as Landau's equation. The factor α is positive for ordinary flows as is observed in the growth to a constant amplitude. The non-trivial solution of equation 6.4

is:

$$\frac{1}{|A|^2} = \frac{\alpha}{2\gamma_1} + Ce^{-2\gamma_1 t} \tag{6.5}$$

Hence it is clear that $|A|^2$ tends asymptotically to a finite limit:

$$|A|^2_{max} = \frac{2\gamma_1}{\alpha} \tag{6.6}$$

This limit is called a limit cycle. The quantity γ_1 is some function of the Grashof number and near Gr_{cr} it follows that $\gamma_1(Gr_{cr}) = 0$ and the zero order term in the expansion is equal to zero, resulting for the first order approximation: $\gamma_1 = C(Gr - Gr_{cr})$. Substituting this into 6.6 we see:

$$|A|_{max} = \sqrt{\frac{2}{\alpha}(Gr - Gr_{cr})} \tag{6.7}$$

This behaviour is known as a Hopf bifurcation. The maximum amplitude is a continuous function of the Grashof number. Therefore it is a supercritical Hopf bifurcation in contrast to a subcritical bifurcation in which hysteresis plays a role and the branching is discontinuous. In a figure displaying the phase of the flow (like figure 6.10) a Hopf bifurcation is the evolution of a point to a small circle.

A Hopf bifurcation is also observed in the simulations as described in section 6.1. This can be shown in a bifurcation diagram as given in figure 6.13 and 6.14 for the mentioned simulations. From this figure the critical Grashof number can be determined by matching α

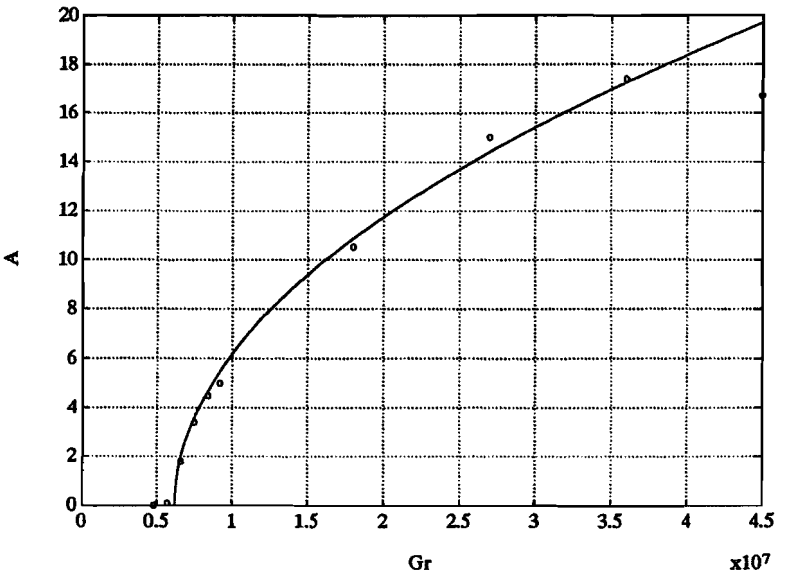

Figure 6.13: Bifurcation diagram for simulated flows; Amplitude

with the simulations and equation 6.7. It turns out to be that $Gr_{cr} \approx 6.2 \cdot 10^6$ for $\alpha = 2 \cdot 10^{-5}$.

Because of the first order expansion equation 6.7 is only valid near to Gr_{cr} and at higher values probably a new critical Grashof number is exceeded. Another bifurcation has taken place. For fully developed turbulent flows Landau proposed a route of infinite number of Hopf

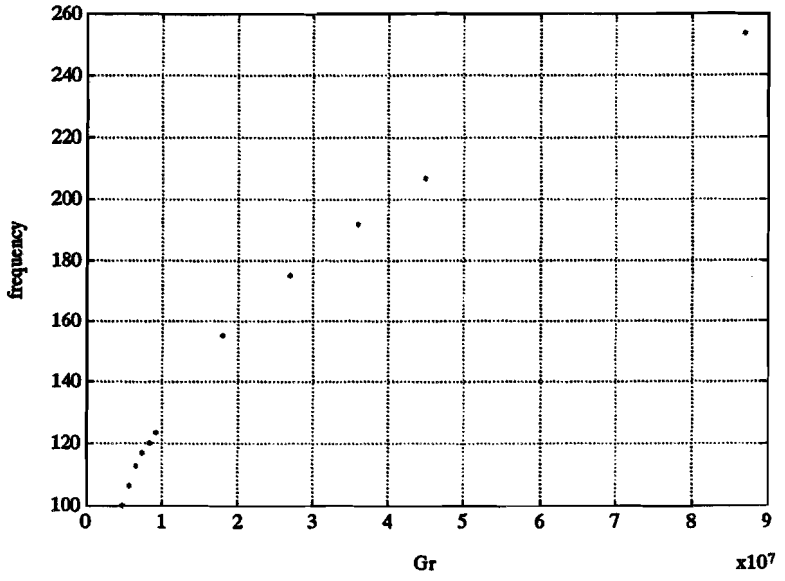

Figure 6.14: Bifurcation diagram for simulated flows; Frequency

bifurcations. This route to chaos, as it is called generally, has never been observed. However for one-dimensional systems with a quadratic nonlinearity Feigenbaum [11] has proved this scenario to be true, as also observed in experiments. From their study of dynamical systems Newhouse, Ruelle and Takens [27] conclude that after two bifurcations a non-periodic flow may appear (see also [35]). The time dependence of the flow then becomes chaotic with sensitive dependence on initial conditions. Amongst other observations this route is experimentally observed for Rayleigh-Bénard convection by Gollub and Benson [15] amongst others. In this experiment also the bifurcation sequence of Feigenbaum was observed by Libchaber and Maurer, see [11], see also Frøyland [12].

6.4 The differentially heated cavity

To look somewhat closer to some aspects of the calculations that can be performed with the present numerical code the flow in a differentially heated cavity was simulated. There is very much known about this configuration and the effect of the subgrid scale model on both the laminar velocity profiles as well as on the transition can be studied. The cavity is a cubical box differentially heated over two opposite vertical walls by prescribing the temperature at it. A no-slip condition was applied at the mentioned walls and at the top and bottom walls of the flow domain. The simulations were performed for laminar two-dimensional flows on a $18 \times 6 \times 18$-grid. The boundary conditions at the front and back were taken periodic to preserve two-dimensionality in the case of stable flows. Adiabatic and conducting top and bottom walls were applied.

The reason for choosing this problem is that the results are easy to compare because of the large amount of investigations involving this case. The work of Henkes [18] is taken here as a reference of comparison. The main attention points of the calculations presented here involve the effect of the subgrid-scale model in laminar flow, the effect of the grid resolution

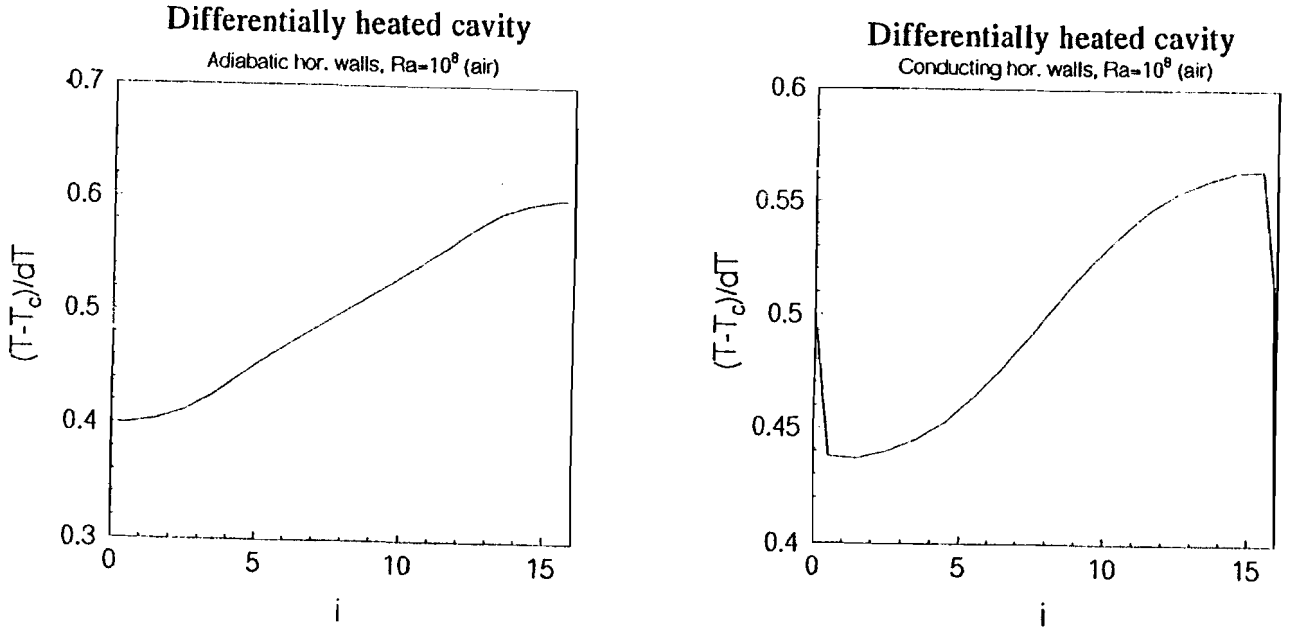

Figure 6.15: Temperature profiles at $x = L/2$, (a) adiabatic (b) conducting case

and the occuring phenomena in the boundary layers where all variables show high gradients.

In the simulations for air at $Gr = 1.4 \cdot 10^8$ with adiabatic horizontal walls it was found that the used grid resolution in the boundary layers was much to poor. The thickness of the vertical velocity boundary layers has to be about $0.05 \cdot L$ where it actually is $0.15 \cdot L$. The proper scalings of the velocities are $\sqrt{g\beta\Delta TL}$ for the vertical direction in the vertical boundary layer and $(g\beta\Delta T\nu)^{1/3}$ for the horizontal direction in the horizontal boundary layers (see Henkes). In this sequence the maximum velocities are 0.11 and 0.86 where they should be 0.27 and 0.82. The largest difference occurs at the vertical walls where the subgrid energy is high. The same calculation was done for water at $Gr = 10^7$ where the dimensionless maximum velocity should be 0.089 and was found to be 0.085.

The temperature profiles (see figure 6.15) were much smoother than the velocity profiles. The large gradient in the conducting case could not be resolved on the given grid. The differences with the mean temperature are too small. For the adiabatic case Henkes [18] gives the same profile but with a difference at the wall of about 0.36 instead of 0.1 of the mean temperature.

Chapter 7

Conclusions and progress

7.1 Conclusions and recommendations

In this study several solution techniques for the flow induced by a horizontal line heat source have been considered. The approach of all methods was to take the Boussinesq approximation as a basic assumption. This may only be done when the temperature differences are small. The use of the Boussinesq approximation is therefore limited by this restriction.

For laminar flow the boundary layer equations, leading to a set of two coupled ordinary differential equations, can be solved numerically using the appropriate boundary conditions. This results in a flow similar to the real flow obtained by experiments. The calculated temperature close to the source however tends to infinity. Also the boundary layer approximation, that assumes a zero momentum exchange in the direction normal to the plume midplane, is not correct, especially in this area. Therefore the obtained solutions are only valid at relative large distances above the source. Using linear stability theory the neutral stability curve can be calculated. This gives a good agreement with experiments when stable and amplified frequencies are compared. From visual observations the begin and end of transition for air were determined to be at approximately $Gr_x = 6.4 \cdot 10^6$ and $Gr_x = 2.95 \cdot 10^7$ respectively. Here boundary layer theory gives rather low and unrealistic predictions for the critical values of x. An integral method is able to describe the macroscopic time mean features of a fully developed turbulent plume.

In this study large eddy simulations have been performed to obtain time dependent solutions. In all cases, however, the mesh was too course, especially in the near wall regions, even in the laminar case. Yet it seems to be possible to obtain a qualitative prediction of a laminar to turbulent transition, both in spatial and temporal sense. It is not known how much the subgrid scale model damps laminar flow, postpones temporal transition and spreads a sharp spatial transition.

In the simulated laminar convection flows the resolution of the grid in the wall regions was too low to solve the flow accurately. If flows are simulated in which the domain is bounded by walls and the phenomena happening in these regions influence the interior at an impermissible level, something has to be done to raise accuracy. The applicable tools are equidistant grid refinement, local grid refinement and the use of wall functions. Because of the lack of computer capacity equidistant refinement is not possible. On the other hand the use of wall functions is limited because of its dependence on the vigor of the flow, that can vary in time and in space and depends highly on the flow configuration under consideration.

Using local grid refinement Henkes [18] obtained accurate results for laminar flow in a cavity at high Grashof numbers with a limited gridsize (30×30).

The damping in laminar flows caused by the subgrid scale model is not investigated yet. This could be done by comparison with a direct simulation. Also the delay of bifurcations with increasing Grashof numbers caused by this effect has to be examined in the same way.

An important effect occuring in laminar natural convection flows that has to be taken into account is the non-uniqueness as reported by Gollub and Benson [15]. This effect probably can influence the route to fully developed turbulence dramatically.

The first time dependence occuring in the simulated flows is in agreement with theoretical analysis resulting in a prediction of a Hopf bifurcation. As stated above it has to be investigated whether this happens at the right critical Grashof number. Further bifurcations leading to turbulent flow qualitatively seem to be in agreement with the routes measured by Gollub and Benson [15] and predicted by Newhouse, Ruelle and Takens [27] in which few bifurcations are preceeding a broadband spectrum. The accuracy of the spatial structure of the laminar to turbulent transition must be examined by comparison with experiments of statistical stationary turbulent plumes and numerical solutions obtained with a refined mesh.

Furthermore turbulent spectra of velocity and temperature have to be measured in a flow configuration that can be simulated and must be compared with calculations. The Nusselt number, a quantity denoting the total energy transfer, has to be compared under several circumstances to get an integral rating of the performance of the numerical code.

Care has to be taken with respect to the dimensions of the flow domain and the choice of the boundary conditions. With respect to the flow domain it was observed that instationary motions could not damp out in more or less cubical configurations. The influence of these motions was felt in the full flow domain. In this case there was no abrubt spatial transition of the flow. Application of periodic boundary conditions can lead to a net mass flux through the domain that can not be achieved experimentally.

To extend the simulations to flows in a more complex geometry it must be investigated how the subgrid scale models can be implemented in finite element methods or spectral element methods, e.g. Sepran. Also finite difference and finite volume methods with general coordinate transformations, e.g. ISNaS, can be applied. Further on a study has to be carried out whether there exist subgrid scale models that are based on a wave number description of the turbulence and are suited for use in natural convection problems. In this case it is interesting to use a spectral element method because of its natural spectral cut-off in wave number space, which is in agreement with the basic idea of modelling in large eddy simulation. Simplicity of the model as well as a good representation of physical reality could be achieved in this way.

Besides these aspects it has to be found out what boundary conditions can be applied within the different numerical codes. Since the governing equations are elliptical, boundary conditions influence the full flow domain. This is important for the accuracy of simulations, especially in regions near boundaries. Interesting questions in this perspective are what to do in near-wall regions and how to define in- and outflow conditions at the numerical boundaries of free convection flows. Outflow conditions must allow phenomena generated in the computational domain to pass through the boundary without undergoing significant distortion and without influencing the interior solution.

At the moment when it is possible to solve the flows of interest with convenient accuracy design criteria can be tested numerically and we are a step closer to the deduction of designing rules. Finally model coefficients of turbulence models (like models based on Reynolds aver-

aging, e.g. the k-ϵ-model) that can be used in low computational effort consuming numerical codes could be tuned.

7.2 Progress

As suggested in the previous section several comparisons of calculations with experiments have to be carried out. A first proposal is to look at the flow induced by a line heatflux source embedded in or lifted above an isothermal lower wall of a perfect cubical domain and bounded by walls at all sides. All other walls are adiabatic except for the lower wall. At moderate Grashof numbers in the statistical stationary case the mean flow structure, some velocity and temperature frequency spectra and the Nusselt number have to be determined.

Experimentally the flow is relative easy to attain. Only the energyflux through the walls has to be controlled. Because the simulations are based on the Boussinesq approximation the experiment has to be designed to not violate this approximation too much, i.e. temperature differences have to be kept small, length scales are therefore large given a specific fluid.

In the numerical simulations the gridsize has to be estimated. The accuracy obtained in calculations with the estimated gridsize can be tested by grid refinement. Eventually a local grid refinement could be applied. Eventually a direct numerical simulation could be performed.

For qualitative comparison eventually physical and numerical shadowgraphs or Schlieren techniques as applied by Comte [6] can be used.

At this moment it is not clear whether the spatial and temporal transition to turbulence obtained with the employed subgrid energy model is in good agreement with physical reality. For numerical comparison other subgrid scale models have to be integrated in the numerical code. First a Smagorinsky [40] model and a vorticity model, which are very similar, have to be built in. This as a first step to the use of the dynamical model of Germano et al. [14] that has to be applied to examine the improvement of this model on the transition. Further on the structure function model of Métais and Lesieur [26] could be used. With these variations of subgrid scale stress closures the energy closure has to be remained constant. In this way the best stress closure can be determined and a variation of the Grashof number has to be carried out to ascertain the general applicability of the model. The first step that is recommended in this comparison is the simulation of a well defined laminar flow, e.g. the differentially heated cavity. Also statistically non-steady flows, for example the starting behaviour and temporal transition, have to be studied. This because in the first place these phenomena occur in practice and secondly they can influence the statistically steady solution.

An interesting case that eventually could be simulated then is the spreading of turbulent plane plumes. The problem is well defined and it can serve to obtain experience with open boundary conditions. It can be simulated by placing the heat source in the interior of the domain and applying inflow and outflow conditions at the bottom and top. For the inflow the pressure has to be described and for the outflow the Orlanski [29] boundary condition can be applied. Having obtained a stationary solution the simulation could be continued with the top of the original domain (excluding the heat source), using open boundary conditions for the top and (new defined) bottom. Similar methods were succesfully used for the mixing layer and the wake behind a sphere [5]. The spreading rate can be compared to those that are obtained from integral methods and experiments in "unbounded" space. Also coherent structures can be examined.

Because it is our aim to solve turbulent natural convection flows in complex geometries we have to apply a coordinate transformation, that leads also to a transformation of the governing equations. Therefore it is easier to investigate whether the closure models can be applied in other numerical methods like another finite volume method, e.g. ISNaS, a finite element method, e.g. Sepran, or a spectral element method. Then using one of these methods interesting flows in rather arbitrary geometries can be solved. The ISNaS code uses a coordinate transformation to obtain a mathematical domain with nice properties in which the calculations can be performed [41]. A disadvantage is the fact that the equations have to be transformed as well. This results in the appearance of extra terms. The advantage of finite element and spectral element methods is that this does not occur. Both finite and spectral element methods use basis functions to represent the variables [7], [42]. These functions are given by ordinary polynomials and Jacobi polynomials respectively. The most commom used Jacobi polynomials are Legendre and Chebyshev polynomials. This means that the suggested advantage of a natural definition of the spectral cut-off as in the Fourier space can not be obtained with the spectral element method. However, the advantage of spectral element methods is the (spectral) accuracy that can be met at constant computer effort in comparison with the other two methods. To the author's opinion the ISNaS code provides the simplest base to implement a subgrid scale model. This was already done by Vreman [44] for compressible flows in a case where there was no transformation required. Therefore ISNaS is the most recommended code to use, when a three dimensional version is available.

References

[1] R. Asselin. Frequency filter for time integrations. *Monthly Weather Rev.*, 100:487–490, 1972.

[2] R.G. Bill Jr. and B. Gebhart. The transition of plane plumes. *Int. J. Mass Heat Transfer*, 18:513–526, 1975.

[3] J.P. Chollet and M. Lesieur. Parametrization of small scales of three-dimensional isotropic turbulence utilizing spectral closures. *J. Atmos. Sci.*, 38:2747–2757, 1981.

[4] R.A. Clark, J.H. Ferziger, and W.C. Reynolds. Evaluation of subgrid-scale models using an accurately simulated turbulent flow. *J. Fluid Mech.*, 91 part 1:1–16, 1979.

[5] P. Comte, August 1992. Private communication.

[6] P. Comte. Visualization of turbulent coherent structures in numerical wind tunnels. In *Summercourse on principles of visualization in fluid mechanics.* J.M. Burgers centre for fluid mechanics, August 1992.

[7] C. Cuvelier, A. Segal, and A.A. van Steenhoven. *Finite element methods and Navier Stokes equations.* D. Reidel Publishing Co. Dordrecht/Boston/Lancastor/Tokyo, 1986.

[8] J.W. Deardorff. A numerical study of three-dimensional turbulent channel flow at large Reynolds numbers. *J. Fluid Mech.*, 41:453–480, 1970.

[9] J.W. Deardorff. Three-dimensional numerical modeling of the planetary boundary layer. In D.A. Haugen, editor, *Workshop on micrometeorology*, chapter 7, pages 271–311. American meteorological society, 1973.

[10] T.M. Eidson. Numerical simulation of the turbulent Rayleigh-Bénard problem using subgrid modelling. *J. Fluid Mech.*, 158:245–268, 1985.

[11] M.J. Feigenbaum. Universal behavior in nonlinear systems. *Physica*, 7D:16–39, 1983.

[12] J. Frøyland. *Introduction to chaos and coherence.* IOP Publishing Ltd., 1992.

[13] B. Gebhart, L. Pera, and A.W. Schorr. Steady laminar natural convection plumes above a horizontal line heat source. *Int. J. Heat Mass Transfer*, 13:161–171, 1970.

[14] M. Germano, U. Piomelli, P. Moin, and W.H. Cabot. A dynamical subgrid-scale eddy viscosity model. *Phys. Fluids A*, 3(7):1760–1765, 1991.

[15] J.P. Gollub and S.V. Benson. Many routes to turbulent convection. *J. Fluid Mech.*, 100(3):449–470, 1980.

[16] D.D. Gray and A. Giorgini. The validity of the Boussinesq approximation for liquids and gases. *Int. J. Heat Mass Transf.*, 19:545–551, 1976.

[17] F.H. Harlow and J.E. Welch. Numerical calculation of time-dependent viscous incompressible flow of fluid with free surface. *The Physics of Fluids*, 8(12):2182–2189, 1965.

[18] R.A.W.M. Henkes. *Natural-convection boundary layers.* PhD thesis, Delft Univerity of Technology, the Netherlands, 1990.

[19] Y. Jaluria. Thermal plumes. In S. Kakaç, W. Aung, and R. Viskanta, editors, *Natural convection; fundamentals and applications*, pages 51–74. Hemisphere Publishing Corporation, 1985.

[20] A.N. Kolmogorov. The local structure of turbulence in incompressible viscous fluid for very large Reynolds numbers. *Dokl. Akad. Nauk SSSR*, 30:301–305, 1941.

[21] P. de Korte, J.G.M. Eggels, and F.T.M. Nieuwstadt. The influence of the initial conditions on freely decaying isotropic turbulence. *Delft progr. rep.*, 15:103–122, (1991-1992).

[22] N.E. Kotsovinos. Turbulence spectra in free convection flow. *Phys. Fluids A*, 3(1):163–167, 1991.

[23] D. Kwak, W.C. Reynolds, and J.H. Ferziger. *3-D time dependent computation of turbulent flows.* Rep. TF-5, Dept. Mech. Eng. Stanford University, 1975.

[24] L.D. Landau and E.M. Lifshitz. *Fluid mechanics.* Course of theoretical physics. Pergamon Press, 1959.

[25] A. Leonard. Energy cascade in large-eddy simulations of turbulent fluid flows. *Adv. in Geophys.*, A18:237–248, 1974.

[26] O. Métais and M. Lesieur. Spectral large-eddy simulation of isotropic and stably stratified turbulence. *J. Fluid Mech.*, 239:157–194, 1992.

[27] S. Newhouse, D. Ruelle, and F. Takens. Occurence of strange axiom A attractors near quasi periodic flows on $T^m, m \geq 3$. *Commun. math. Phys.*, 64:35–40, 1978.

[28] F.T.M. Nieuwstadt. Direct and large-eddy simulation of free convection. In *Proc. 9^{th} Internat. Heat Transfer Conf., Jerusalem 19-24 August 1990*, pages 37–47. Amer. Soc. Mech. Eng., New York, 1990.

[29] I. Orlanski. A simple boundary condition for unbounded hyperbolic flows. *J. Comp. Phys.*, 21:251–269, 1976.

[30] L. Pera and B. Gebhart. On the stability of laminar plumes: some numerical solutions and experiments. *Int. J. Heat Mass Transfer*, 14:975–984, 1971.

[31] S.A. Piacsek and G.P. Williams. Conservation properties of convection difference schemes. *J. Comp. Phys.*, 6:392–405, 1970.

[32] M.J.B.M. Pourquié. Stability analysis for the large eddy models in rectangular and cylindrical coordinates. Technical report, Delft University of Technology, the Netherlands, 1991.

[33] R.S. Rogallo and P. Moin. Numerical simulation of turbulent flows. *Ann. Rev. Fluid Mech.*, 16:99–137, 1984.

[34] H. Rouse, C.S. Yih, and H.W. Humphreys. Gravitational convection from a boundary source. *Tellus*, 4:201–210, 1952.

[35] D. Ruelle and F. Takens. On the nature of turbulence. *Commun. math. Phys.*, 20:167–192, 1971.

[36] H. Schmidt and U. Schumann. Coherent structure of the convective boundary layer derived from large eddy simulation. *J. Fluid Mech.*, 200:511–562, 1989.

[37] U. Schumann. Subgrid scale model for finite difference simulations of turbulent flows in plane channels and annuli. *J. Comp. Phys.*, 18:376–404, 1975.

[38] J.J.M. Sillekens. Mixed forced and buoyancy-induced convection in a square channel: governing equations and approximations. Technical report, Eindhoven University of Technology, the Netherlands, 1992.

[39] A. Silveira Neto, D. Grand, O. Métais, and M. Lesieur. Large-eddy simulation of the turbulent flow in the downstream region of a backward-facing step. *Phys. Rev. Letters*, 66(18):2320–2323, 1991.

[40] J. Smagorinsky. General circulation experiments with the primitive equations. *Mon. Weather Rev.*, 91(3):99–165, 1963.

[41] H.P. Sparidans. De ISNaS incompressible flow solver. Technical Report WOC WET 92.010, Eindhoven University of Technology, the Netherlands, 1992. In Dutch.

[42] L.J.P. Timmermans, J.K.M. Jansen, and F.N. van de Vosse. A description of the fundamentals of the spectral element method. Technical Report WFW - report 90.041, Eindhoven University of Technology, the Netherlands, 1990.

[43] T.A.M. Versteegh and F.T.M. Nieuwstadt. Numerical simulation of buoyancy driven flows in enclosures. To be published in the proceedings of the meeting-workshop "on Mixing in Geophysical Flows, Effects of Body forces in Turbulent Flows", Barcelona, December 1992.

[44] A.W. Vreman, B.J. Geurts, J.G.M. Kuerten, and P.J. Zandbergen. A finite volume approach to large eddy simulation of compressible, homogeneous, isotropic, decaying turbulence. *Int. J. for Num. Meth. in Fluids*, 15:799–816, 1992.

Appendix A

Approximation of the similarity functions

To determine the velocity profiles and fringe patterns the similarity functions are approximated by Gaussian distributions for f' and ϕ, using the values at $\eta = 0$ obtained by Pera and Gebhart [30], so that only the width had to be fitted:

$$f'(\eta) = 0.6618e^{-0.41\eta^2} \tag{A.1}$$

and

$$\phi(\eta) = e^{-0.43\eta^2} \tag{A.2}$$

Equation A.1 results in an error function for f, given by:

$$f(\eta) = 0.9160\text{erf}(0.6403\eta) \tag{A.3}$$

Plots of these approximations are presented in figure A.1.

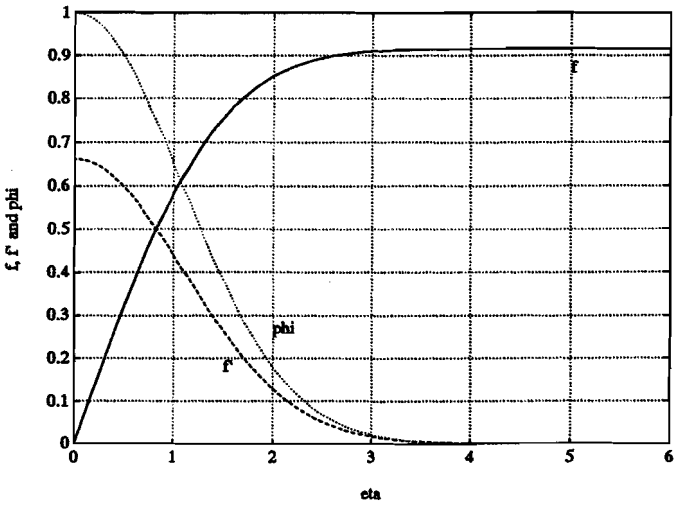

Figure A.1: Approximated similarity functions

Appendix B

Some velocity time series

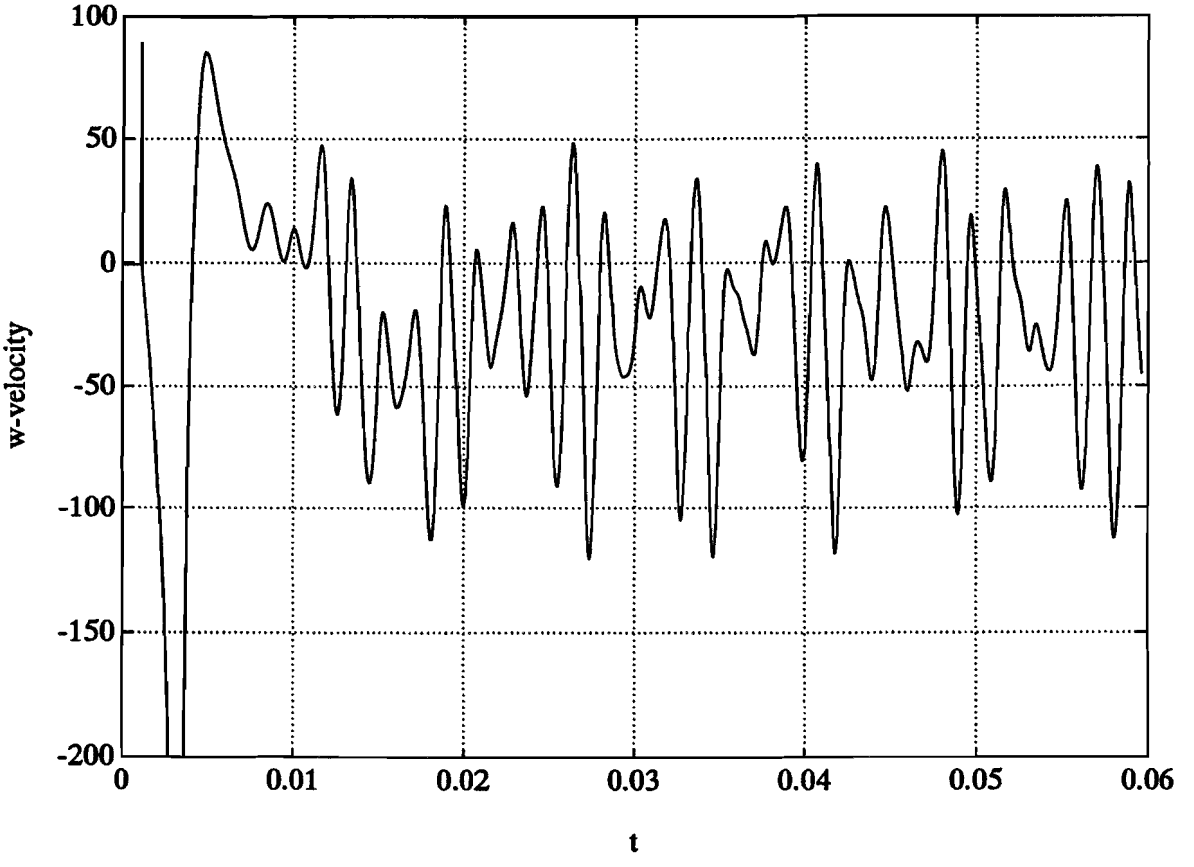

Figure B.1: Detailed velocity presentation for $Gr = 8,6 \cdot 10^8$

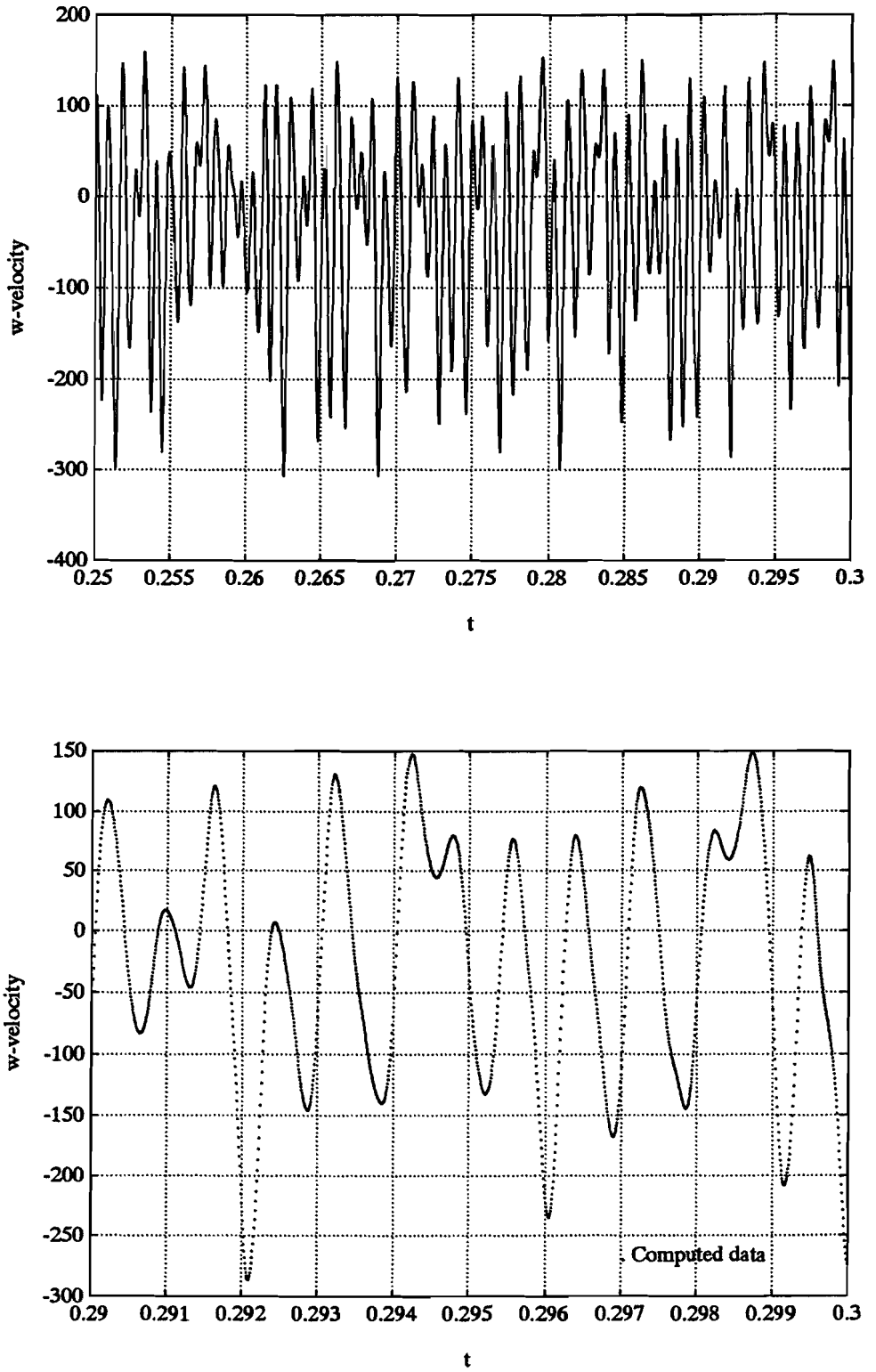

Figure B.2: Detailed velocity presentation for $Gr = 8,4 \cdot 10^9$

Appendix C

Velocity time series and frequency spectra

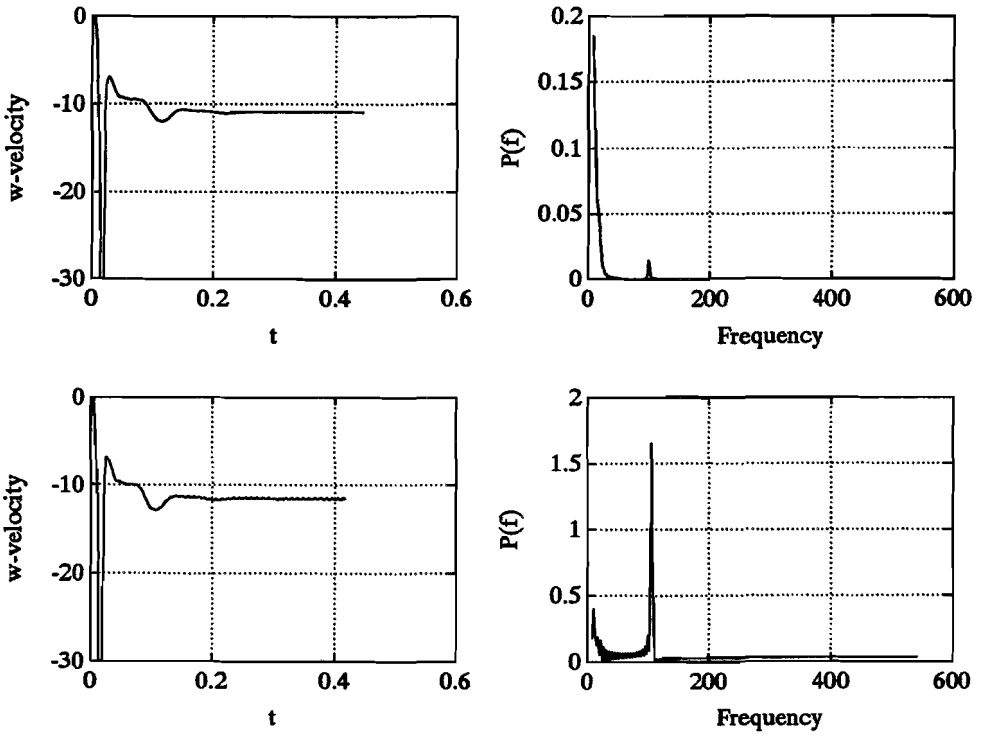

Figure C.1: $w(50,6,6,t_i)$ *and* $P(50,6,6,f)$ *at* $Gr = 4.8 \cdot 10^6$ *and* $Gr = 5.7 \cdot 10^6$

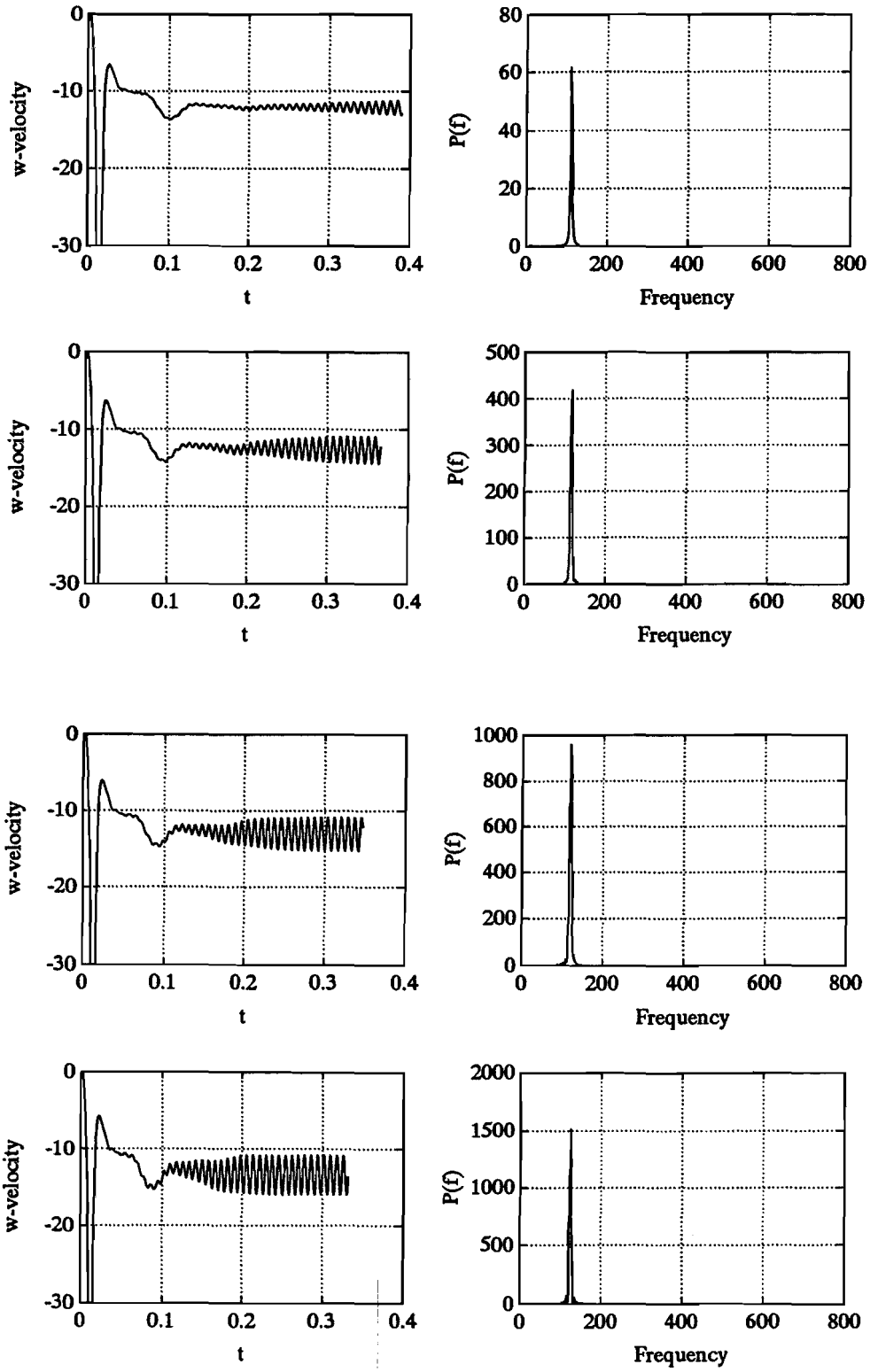

Figure C.2: $w(50, 6, 6, t_i)$ *and* $P(50, 6, 6, f)$ *at* $Gr = 6.6 \cdot 10^6$, $Gr = 7.5 \cdot 10^6$, $Gr = 8.4 \cdot 10^6$ *and* $Gr = 9.2 \cdot 10^6$

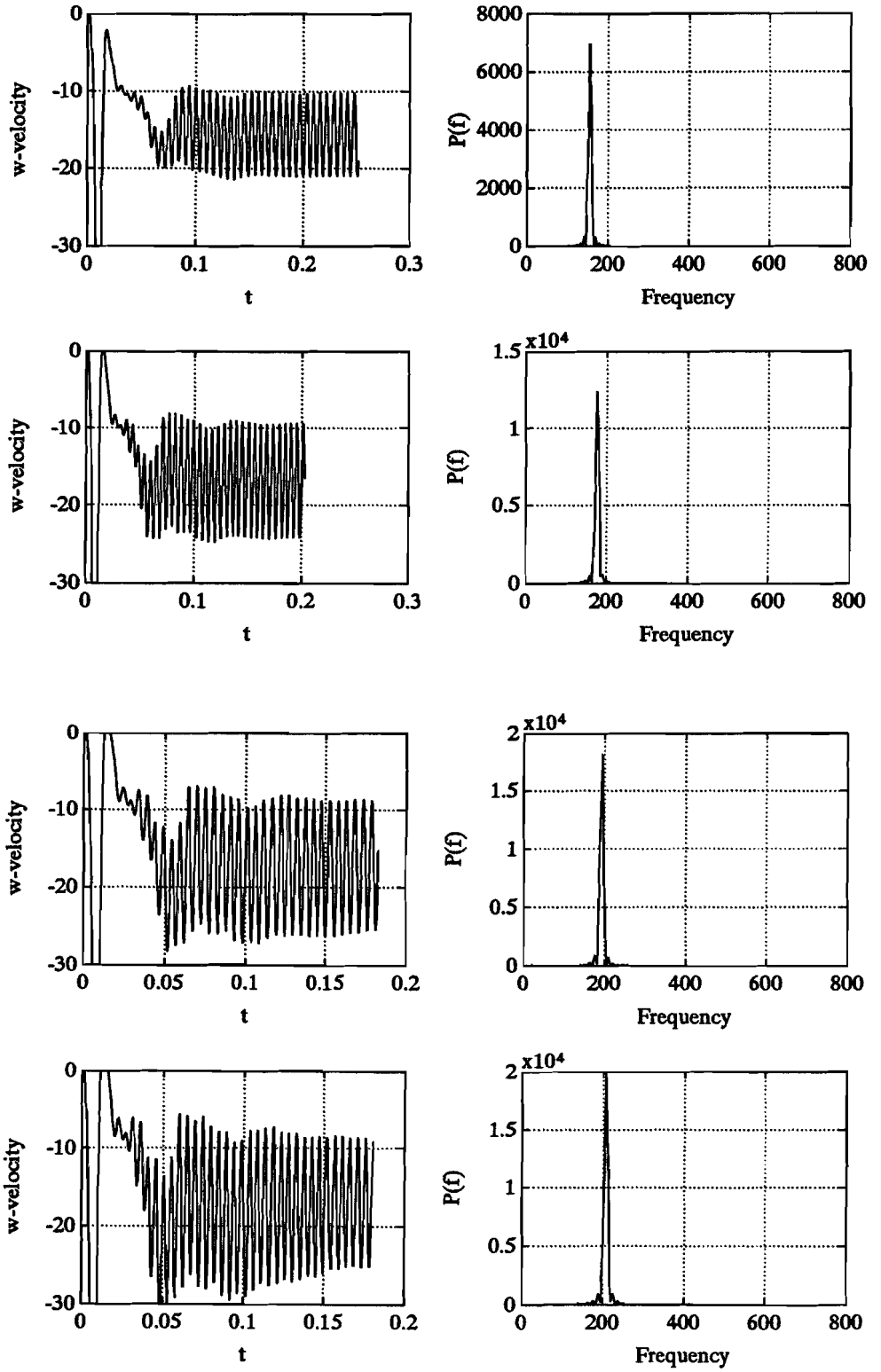

Figure C.3: $w(50, 6, 6, t_i)$ *and* $P(50, 6, 6, f)$ *at* $Gr = 1.8 \cdot 10^7$, $Gr = 2.7 \cdot 10^7$, $Gr = 3.6 \cdot 10^7$ *and* $Gr = 4.5 \cdot 10^7$

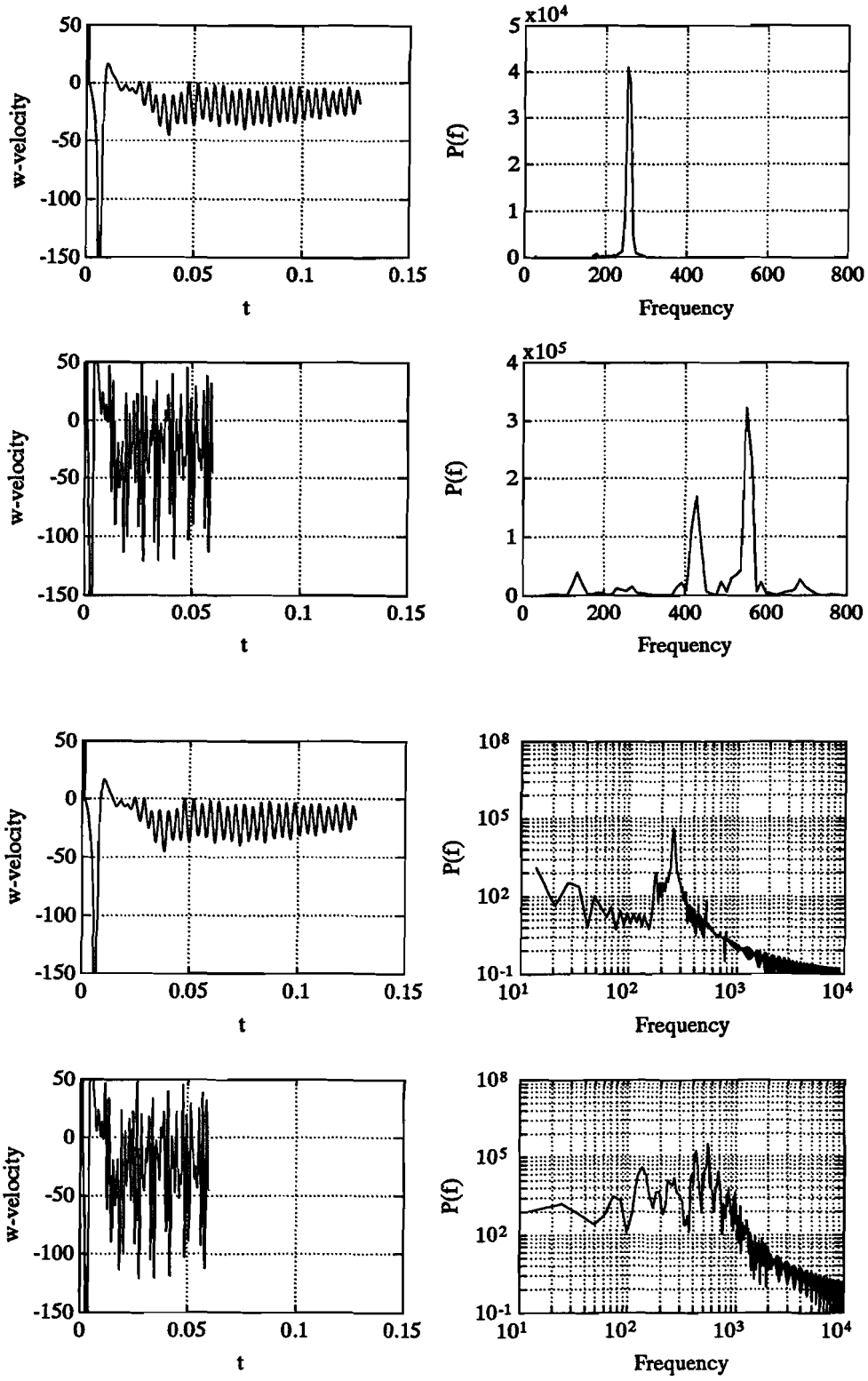

Figure C.4: $w(50,6,6,t_i)$ and $P(50,6,6,f)$ at $Gr = 8.7 \cdot 10^7$, and $Gr = 8.6 \cdot 10^8$, linear and double logarithmic spectrum

Appendix D

The differential equation for the subgrid energy

To determine the eddy coefficients a differential equation for the subgrid energy is used. This equation is formulated in terms of the square root of the subgrid energy $\sqrt{e}$, the quantity needed to determine the eddy diffusivity (equation 5.11):

$$\frac{\partial}{\partial t}e^{1/2} + \frac{\partial}{\partial x_j}(\overline{u}_j e^{1/2}) = \frac{\partial}{\partial x_j}\left(\nu_T \frac{\partial}{\partial x_j}e^{1/2}\right) + \frac{2\nu_T \overline{S}_{ij}\frac{\partial \overline{u}_i}{\partial x_j} + \frac{1}{2}\nu_H \frac{g_i}{T_0}\frac{\partial^2 \overline{T}}{\partial x_i^2}}{2e^{1/2}} - \frac{1}{2}C_d\frac{e}{\Delta} \qquad \text{(D.1)}$$

Equation D.1 was used in the preliminary calculations as presented in this report. It has to be noted that there are some errors in it. The correct subgrid energy equation (see also Versteegh and Nieuwstadt [43]) should read:

$$\frac{\partial e}{\partial t} + \frac{\partial}{\partial x_j}(\overline{u}_j e) = \frac{\partial}{\partial x_j}\left(\nu_H \frac{\partial e}{\partial x_j}\right) + 2\nu_T \overline{S}_{ij}\frac{\partial \overline{u}_i}{\partial x_j} + \nu_H g_i \beta \frac{\partial \overline{T}}{\partial x_i} - C_d\frac{e^{3/2}}{\Delta} \qquad \text{(D.2)}$$

It is assumed that the diffusion coefficient of subgrid energy is equal to the diffusivity of temperature (diffusion of a scalar). According to Schmidt and Schumann [36] the constant C_d must be taken equal to 0.7 (see also de Korte et al. [21]). The first source term accounts for the rate of irreversible turbulent conversion to internal energy. An extra source term is introduced to deal with the damping effect of a stable vertical temperature stratification and can be found by dimensional analysis. In this case it is negative and it removes subgrid energy. When there is an unstable stratification it is assumed that the temperature gradient dies out very fast by convection and the term will not affect the solution in a significant way. The sink term can be derived from the assumption that the spectral cut-off of the used filter lies in the inertial subrange.

The differences between the two expressions are concerning the diffusion and the stratification term. The stratification term of D.1 is multiplied by a half and it contains the second derivative of the temperature. Also the ideal gas law was used in this formulation, whereas, with the use of the expansion coefficient, equation D.2 is more general applicable. The diffusion term of subgrid energy in the former equation has to be divided by a factor $2\sqrt{e}$, making advection more important. Furthermore it can be argued that the use of temperature diffusivity is a better approximation for the coefficient.

In the future the last equation will be applied. It is assumed however that the preliminary calculations are not affected too much, especially as regards the qualitative results.